Full-length Article

Intranasal delivery of SARS-CoV-2 spike protein is sufficient to cause olfactory damage, inflammation and olfactory dysfunction in zebrafish

Aurora Kraus [a], Mar Huertas [b], Laura Ellis [b], Pierre Boudinot [c], Jean-Pierre Levraud [d], Irene Salinas [a,*]

[a] Center of Evolutionary and Theoretical Immunology, Biology Department, University of New Mexico, NM, USA
[b] Department of Biology, Texas State University, San Marcos, TX, USA
[c] Université Paris-Saclay, INRAE, UVSQ, VIM, 78350 Jouy-en-Josas, France
[d] Unité Macrophages et Développement de l'Immunité, Institut Pasteur, CNRS UMR3637, Paris, France

ARTICLE INFO

ABSTRACT

Anosmia, loss of smell, is a prevalent symptom of SARS-CoV-2 infection. Anosmia may be explained by several mechanisms driven by infection of non-neuronal cells and damage in the nasal epithelium rather than direct infection of olfactory sensory neurons (OSNs). Previously, we showed that viral proteins are sufficient to cause neuroimmune responses in the teleost olfactory organ (OO). We hypothesize that SARS-CoV-2 spike (S) protein is sufficient to cause olfactory damage and olfactory dysfunction. Using an adult zebrafish model, we report that intranasally delivered SARS-CoV-2 S RBD mostly binds to the non-sensory epithelium of the olfactory organ and causes severe olfactory histopathology characterized by loss of cilia, hemorrhages and edema. Electrophysiological recordings reveal impaired olfactory function to both food and bile odorants in animals treated intranasally with SARS-CoV-2 S RBD. However, no loss of behavioral preference for food was detected in SARS-CoV-2 S RBD treated fish. Single cell RNA-Seq of the adult zebrafish olfactory organ indicated widespread loss of olfactory receptor expression and inflammatory responses in sustentacular, endothelial, and myeloid cell clusters along with reduced numbers of T_{regs}. Combined, our results demonstrate that intranasal SARS-CoV-2 S RBD is sufficient to cause structural and functional damage to the zebrafish olfactory system. These findings may have implications for intranasally delivered vaccines against SARS-CoV-2.

1. Introduction

Smell critically influences animal behavior and survival (Kermen et al., 2013; Kraus et al., 2021; Meisel and Kim, 2014; Stensmyr et al., 2012). A hallmark of SARS-CoV-2 infection is acute loss of smell, or anosmia (Carignan et al., 2020; Chung et al., 2020; Cooper et al., 2020; Eliezer et al., 2020; Gorzkowski et al., 2020). While most COVID-19 patients who report anosmia begin olfactory recovery by 2 weeks after onset, a small percentage, (~5%) report lingering smell impairment after a month (Gorzkowski et al., 2020). Further, anosmia is linked to worse clinical outcome of COVID-19 patients admitted to hospital with acute respiratory distress syndrome (Mangia et al., 2021).

Viral-induced anosmia is not unique to SARS-CoV-2 infections; other respiratory viruses such as rhinoviruses, influenza, parainfluenza and seasonal coronaviruses cause olfactory deficits in humans (Imam et al., 2020; Suzuki et al., 2007). While the precise mechanism of anosmia in

COVID-19 patients is unclear, a range of potential explanations have been posited. First, viral induced anosmia may be due to inflammatory obstruction of the nasal cavities. In support, COVID-19 patients have increased pro-inflammatory cytokine levels in their olfactory epithelium (OE) (Rodriguez et al., 2020; Torabi et al., 2020). In mouse OE, sterile induction of type I IFN leads to widespread loss of olfactory receptor (OR) expression, indicating that olfactory dysfunction can be caused by inflammation even in the absence of active viral replication (Rodriguez et al., 2020). However, a significant number of COVID-19 patients report anosmia uncoupled from nasal cavity swelling (Chung et al., 2020; de Melo et al., 2021a; Gorzkowski et al., 2020) and therefore further studies are warranted. Second, SARS-CoV-2 infection of supporting cells may secondarily damage olfactory sensory neurons (OSNs) and therefore compromise the transduction of chemical odorant information to the olfactory bulb (OB) (Cooper et al., 2020). In mice and humans, *ace2* expression is detected in sustentacular cells (SCs), olfactory stem cells

---

and perivascular cells (pericytes) in the OB, but not OSNs (Brann et al., 2020; Chen et al., 2021; Sungnak et al., 2020). Further, in human biopsies, viral RNA is detected in the lamina propria of the olfactory organ (OO) and in SCs indicating infrequent infection of OSNs (Zazhytska et al., 2021). Furthermore, infection of golden Syrian hamsters with SARS-CoV-2 results in infection of a large proportion of SC but not OSNs, yet OSNs are damaged as evidenced by the major loss of cilia (Bryche et al., 2020). Combined, it appears that infection of SCs by SARS-CoV-2 alters the local metabolic and inflammatory state of the whole OO resulting in damage to the OSNs and subsequent anosmia (Brann et al., 2020; Dias De Melo et al., 2021b).

The SARS-CoV-2 Spike (S) protein is a homotrimer and each monomer is comprised of a S1 subunit and a S2 subunit (Lan et al., 2020). The S1 subunit includes an N-terminal domain and the receptor binding domain (RBD). SARS-CoV-2 S RBD binds to angiotensin-converting enzyme 2 (ACE2) on a permissive host cell, then a serine protease, such as TMPRSS2, cleaves the spike protein S1/S2 site to facilitate fusion of the virion with the host cell membrane (Hoffmann et al., 2020b; Hoffmann et al., 2020a). Once RBD binds ACE2, endocytosis of the complex occurs. Once inside the cell, S protein may be degraded and release of free S protein fragments from infected cells may occur. In fact, it has been hypothesized that infected cells and virions shed free soluble S1 subunits that can bind ACE2 and result in downstream deleterious effects and inflammation (Letarov et al., 2021). Although this hypothesis requires further experimental support, viral-derived proteins such as glycoproteins from coronaviruses and HIV have been shown to induce an IFN response in peripheral blood cells (Ankel et al., 1994; Laude et al., 1992). Further, neuroinflammatory responses to viral proteins, even in the absence of an active infection, have been documented (Bansal et al., 2000; Holz et al., 2017; Rhea et al., 2021). For instance, we have shown that the glycoprotein (G protein) of infectious hematopoietic necrosis virus is sufficient to trigger nasal neuroimmune responses in teleost fish (Sepahi et al., 2019). Based on this body of work, we hypothesized that SARS-CoV-2 S RBD protein is sufficient to cause olfactory pathology and dysfunction.

The zebrafish olfactory system shares a significant degree of molecular and anatomical conservation with humans (Saraiva et al., 2015). The zebrafish OO consists of two separate rosettes exposed to the external environment where the OSNs directly detect chemical stimuli in the environmental water. Rosettes are formed by many olfactory lamellae, finger-like structures, each coated with non-sensory and sensory neuroepithelium. The sensory regions consist of basal cells, intermediate neuronal precursors, mature OSNs and sustentacular cells, similar to the mammalian OE (Byrd and Brunjes, 1995). OSN axons penetrate the basal lamina in bundles and form the *fila olfactoria* in the lamina propria. In the lamina propria, apart from the OSN axon bundles, fibroblasts, glial cells and blood vessels are found (Hansen and Zeiske, 1998; Sarkar et al., 2018). The zebrafish OO has been extensively studied in different toxicant and injury models (Calvo-Ochoa and Byrd-Jacobs, 2019; Kermen et al., 2013). The regenerative abilities of the OO and OB in zebrafish indicate that the kinetics of anosmic recovery takes about 2 weeks; a similar timeline to that observed in COVID-19 patients who suffer from anosmia (Chung et al., 2020; Gorzkowski et al., 2020; White et al., 2015). Zebrafish offer many advantages over other animal models due to their high reproductive ability, rapid development, low maintenance costs, and small transparent bodies (Levraud et al., 2014). These advantages have already been leveraged to study respiratory and neurotropic human viruses such as Influenza A, noroviruses, Herpes simplex virus and Chikungunya virus (Burgos et al., 2008; Gabor et al., 2014; Palha et al., 2013; Van Dycke et al., 2019). Genetically, more than 80% of disease related genes have a zebrafish orthologue (Howe et al., 2013) and members of all major groups of mammalian cytokines have been identified in the zebrafish genome (Gomes and Mostowy, 2020; Zou and Secombes, 2016).

A few studies have proposed zebrafish as a model for SARS-CoV-2 (Costa et al., 2021; Galindo-Villegas, 2020; Laghi et al., 2021;

Tyrkalska et al., 2021). Attempts to infect wildtype zebrafish larvae by immersion indicate a lack of infection or replication of SARS-CoV-2 (Kraus et al., 2020; Laghi et al., 2021). Microinjection of live SARS-CoV-2 virus into wildtype zebrafish larvae found modest replication in the swim bladder and no replication when microinjected via other routes (Laghi et al., 2021). Thus, at present, the use of wildtype zebrafish (larvae or adults) to understand live SARS-CoV-2 infection is limited. The adult teleost OO has previously been shown to respond to proteins from vial pathogens (Sepahi et al., 2019). Thus, in this study, we investigate the effects of a vial protein, SARS-CoV-2 S RBD protein on the olfactory system of the zebrafish in a BSL-1 setting.

The present study reports for the first time that intranasal (I.N.) delivery of SARS-CoV-2 S RBD is sufficient to cause olfactory pathology in adult zebrafish. The damage was transient, as tissue was repaired by 2 weeks. Electrophysiology further indicate that adult zebrafish have impaired functional responses to odorants after I.N. exposure to SARS-CoV-2 S RBD despite the fact that they did not loose behavioral preference for food odorants. Finally, single cell RNA-Seq indicates global losses in OR expression and decreased numbers of mature OSNs in zebrafish coupled with transcriptional responses in sustentacular, immune and endothelial cells.

2. Materials and methods

2.1. Zebrafish husbandry

Wildtype AB zebrafish were initially obtained from ZIRC (Oregon, USA). For the I.N. delivery of SARS-CoV-2 S RBD protein into adult zebrafish, female and male adult zebrafish were obtained from Dr. Wong's laboratory at the University of Nebraska due to lockdown of ZIRC during the pandemic. Adult male and female OMP:lynRFP zebrafish were kindly shared by Dr. Ankur Saxena and maintained in the same facility as AB animals. Fish were maintained in a filtered aquarium system at 28℃ with a 14 h light and 10 h dark cycle at the University of New Mexico Aquatics Animal Facility. For electro-olfactogram (EOG) recordings, wildtype AB adult zebrafish were obtained from ZIRC and maintained at the TXST Aquatic laboratory in the Freeman building. All experiments with adults utilized a mix of male and female animals. Animals were fed *ad libitum* Gemma complete nutrition (Skretting). All animal protocols were done in accordance with American Veterinary Medical Association guidelines under a protocol approved by the University of New Mexico's Institutional Animal Care and Use Committee (Protocol Number 19–200863-MC) and the Texas State University Institutional Animal Care and Use Committee (Protocol Number 43).

2.2. Comparative analyses of vertebrate ACE2 molecules and RT-qPCR

Primary sequences for ACE2 protein were collected from publicly available databases. Accession number are as follows: *H. sapiens*, Q9BYF1; *M. mulatta*, NP_001129168.1; *M. musculus*, Q8R0I0; *R. norvegicus*, Q5EGZ1; *M. putorius furo*, BAE53380.1; *M. javanica*, XP_017505752.1; *R. sinicus*, U5WHY8; *C. dromedaries*, XP_010991717.1; *C. familiaris*, F1P7C5; *G. gallus*, F1NHR4; *A. mississippiensis*, KYO30243.1; *X. tropicalis*, F6PSC4; *D. rerio*, XP_005169417.1. To assess the similarity and identity of the amino acid sequences we used MatGat v2.02 (Campanella et al., 2003). Alignments were done using CLUSTALW (Chenna et al., 2003).

Olfactory organs and olfactory bulbs were dissected, and RNA was extracted using trizol. For tissue homogenization tungsten beads were placed in 1.5 ml Eppendorf tubes with tissue and trizol and shaken at 30 Hz for 5 min. The homogenate/lysates were then collected, and RNA extracted using a standard chloroform/phenol extraction protocol. Total RNA was quantified by nanodrop and RNA contents were normalized to 0.5 mg prior to reverse transcription to synthesize cDNA using the Superscript III first strand system (Thermofisher 18080051). qPCR was performed using SSOadvanced supermix (Biorad 1725270) using the

following primers: *ace2* forward 5′- CTGGCTCCTGCTTTTGGC-3′ reverse 5′- TCTTTATCTGCATTTTCCTGGGAG-3′ and *rps11* forward 5′- CCCA-GAGAAGCTATTGAT-3′ reverse 5′- TCACATCCCTGAAGCATG-3′ at a Tm of 62. Quantification of changes in gene expression was done by the Pfaffl method (Pfaffl, 2001).

2.3. Intranasal delivery of SARS-CoV-2 S RBD recombinant protein to adult zebrafish

Adult zebrafish were anesthetized for 1 min in 0.04 mg/ml Tricaine-S (Syndel) solution and then moved to an absorbent boat where their gills were still covered with anesthetic solution for administration of solutions to nares. Using a microloader tip (Eppendorf, 930001007), 5 µl of a 20 ng/µl His-tagged SARS-CoV-2 S RBD in PBS (kindly provided by Dr. F. Krammer) was directly pipetted into each naris, while 5 µl of sterile PBS was applied in control fish. For details on production of recombinant SARS-CoV-2 S RBD please refer to Amanat et al., 2020. As a negative control, animals received the same dose of an unrelated His-tagged recombinant protein, the trout chemokine CK12a, a CCL-19 homologue (Sepahi et al., 2017). Additionally, a control treatment group included a single I.N. delivery of 50 µg/naris poly I:C (Sigma Aldrich) or a triple poly I:C delivery consisting of one administration of 50 µg/naris poly I:C daily for 3 days. Fish were sampled 1 day later. As a further positive control for apoptosis assays, the olfactotoxic drug methimazole (Chen et al. 2017, Leung et al., 2007; Suzukawa et al., 2011) or vehicle control was delivered I.N. once (5 µl of a 10 µM methimazole solution in PBS, Millipore Sigma CAS 60–56-0) and animals were sampled a day later. After inoculation, animals recovered in a separate tank supplemented with O_2 before returning to their rearing tank until the end of the experiment. Euthanasia was performed on ice to ensure rapid death without perturbing the olfactory system at 15 min, 3 h, 1 d, 3 d, 5 d and 2 w.

2.4. Histology and image analysis

Adult zebrafish heads ($N = 3$–5) were fixed in 4% formaldehyde solution buffered to pH 7.4 with 60 mM HEPES overnight at 4℃ on a low speed rocker. Heads were then rinsed three times with PBS for 30 min at room temperature (RT) on a slow rocker and decalcified in 10% EDTA solution (pH 7.4) at RT for 24 h. After rinsing in PBS, samples were placed in 70% ethanol for 24 h at 4℃ and then processed for embedding in paraffin according to ZIRC protocols. Paraffin blocks were sectioned at 5-µm thickness and stained by hematoxylin and eosin (H&E) staining or by Masson Trichrome staining (Cancer Diagnostics #SS1026-MAB-500). For histological quantifications, 40x images with pixel ratios of 640x480 were acquired on a Nikon Ti inverted microscope (brightfield) were imported to ImageJ. A distance of 50 µm was measured from where the lamellae meets the raphe and the width of the lamella was measured from basal lamina to basal lamina perpendicular to the lamella. Health of cilia was accessed as previously reported (Casadei et al., 2019; François et al., 2016). In short, areas where the cilia were detached, tangled in knots, or sheared to<1 µm in height were considered unhealthy. The total length of epithelium with healthy cilia was then divided by the total epithelial length to display as "percent of healthy cilia".

For immunofluorescence staining, zebrafish heads ($N = 3$–10) were frozen in OCT (Tissue-Tek, 4583). Sections (5-µm) were post fixed with 4% paraformaldehyde for 3 min and blocked with T20 (Fisher #PI-37539) for 12 min. Sections were then labeled with rabbit anti-6x His (ab9108) (1:300), or mouse anti-PCNA (ab29; PC10) (1:300), or rabbit anti-activated caspase-3 (ab13847) (Jia et al., 2020; Sahoo et al., 2021) (1:300), or mouse anti-cytokeratin 8 (1:250) (Haugarvoll et al., 2008) or corresponding isotype controls followed by secondary antibody labeling with Cy3 donkey anti-mouse (Jackson Immuno Research 715–165-151) or Cy3 goat anti-rabbit (Jackson Immuno Research 111–165-144) or Cy2 goat anti-rabbit (Jackson Immuno research 111–225-144). All

secondaries were used at 1:250. Nuclei were stained with DAPI. Sections were observed under a Nikon Ti inverted microscope, and images were acquired with the Nikon Elements Advanced Research software or on a Zeiss LSM 780 confocal microscope and acquired with Zen software SP4. All images were analyzed using ImageJ. For quantifation of caspase-3 and PCNA, 10 representative images per animal were taken at 60x with a pixel ratio of 1920x1460. All images were acquired with the same exposure time (3 s for caspase-3 and 1 s for PCNA) and LUTs were adjusted to the same level before counting positively stained cells. For the PCNA quantification, only cells with nuclear staining were counted as described by Bettini et al., 2016. Images were taken along the length of the lamella's sensory and non-sensory epithelium. Off target staining and background were determined by isotype controls and ignored for counting. Counting was performed by two scientists independently.

2.5. Isolation of olfactory organ cells from adult zebrafish, scRNA-Seq, scRNA-Seq data analysis and gene ontology

To obtain single cell suspensions, adult AB zebrafish olfactory rosettes ($N = 4$) were dissected and placed directly into 5 ml of Neurobasal medium (Gibco, 21103049) supplemented with 10% heat inactivated fetal bovine serum (FBS, Peak Scientific, Colorado, USA), 100 U/ml penicillin–streptomycin (Gibco, 15140122), and 0.04% filtered bovine serum albumin (Sigma) and rocked at 4℃. Every 20 min, the supernatant from each sample was collected and replaced by fresh medium for a total of 4 times. Supernatants were then filtered through a cell strainer and kept on ice. Next, the rosettes were placed in 10 ml of a DTT solution (1.3 mM EDTA, 864 µM DTT in PBS) at RT for 30 min. Suspensions were filtered through a cell strainer and combined with the supernatants obtained from the first steps. Rosettes were then rinsed off the DTT solution and incubated in Hank's buffer containing 10% FBS, 0.04% BSA, 100U/ml penicillin–streptomycin and collagenase type IV (Gibco, 0.37 mg/ml) for 1.5 h at RT. The supernatants were filtered through a cell strainer and combined with those obtained from the previous steps while the rosettes were mashed against the cell strainer and washed with neurobasal medium. The combined supernatants were centrifuged for 10 min at 400g in supplemented neurobasal medium and cells were counted with a hemocytometer. Viability was estimated by trypan blue staining. Cells were then strained twice through Flowmi 10 µm strainers and loaded onto the chromium controller with a viability of greater than 85%. Cell libraries were generated according to 10x Genomics protocols at the University of New Mexico Cancer Center Genomics core facility and sequenced on an Illumina NovaSeq 6000 at the University of Colorado Genomics and Microarray core facility. Sequencing depth and statistics of the scRNA-Seq run are shown in Figure S9. SRAs for this project can be found on NCBI under bioproject #PRJNA668529.

Fastqs were run through the Cell Ranger v3.0 pipeline with default settings using the GRCz11 zebrafish genome. Output matrices were loaded to R (v1.2.5001) as a Seurat object (Package Seurat v3.1.1). First, cells with<200 or greater than 2500 features, and greater than 5% mitochondrial features were removed. After counts were normalized using the "lognormalize" method and a scale factor of 10000, 2000 variable genes were selected using the 'vst' method. Data was scaled, and PCA dimensional reduction was run. Jackstraw analysis determined the vehicle control to have 38 significant principal components (PCs) and the treated samples to have 40 significant PCs which were used for clustering analysis. SARS-CoV-2 S RBD treated samples were integrated with the vehicle treated sample and clustered together using 30 significant PCs and a resolution of 0.5. Cluster markers were identified with "FindAllMarkers" in Seurat and exported for cluster identification. Differential expression analysis was done with seurat "FindMarkers" in default settings for each cluster and exported for gene ontology analysis.

Gene ontology (GO) analysis was done with web-based GUIs Metascape and ShinyGO v0.61 which draw multiple currently maintained databases (Ensembl, ENTRZ, KEGG among others). Biological process webs were created using biological process output from ShinyGO v0.61

in Prism GraphPad. Biological processes bar graphs were produced by Metascape.

2.6. Electro-olfactogram recordings

Adult AB zebrafish were anesthetized and received 3 μl of recombinant SARS-CoV-2 S RBD protein (50 ng/μl) in PBS, 5 μl r-CK12a protein (50 ng/ml) or PBS alone in the right naris. The left naris always received 5 μl PBS. After 3 h, 1 d, 3 d and 2 w zebrafish were placed in a v-shaped stand and supplied with aerated water containing MS222 anesthetic (0.05 g/L) (Sigma Aldrich) through the gills. The nasal flap was removed with sterile fine forceps to expose the olfactory rosettes to a continuous water line delivered by a microtube on top of the rosette. Olfactory responses to zebrafish food extract or goldfish bile were measured by electrical recordings as detailed in Sepahi et al., 2019. Olfactory responses were recorded first in one naris and then recorded again in the opposite naris, the order of naris to perform EOGs (right-treated naris or left-control naris) was randomized. There were no differences in the olfactory responses between naris due to the order of recording. The food extract was prepared as a filtered solution of 1L tap water and 0.1 g of dry food pellets. Water food extracts were separated in 200 ml aliquots and kept frozen until the recording day. A 0.5 ml mix of bile fluid from 50 adult goldfish was aliquoted in 10 μl and kept frozen until the day of the recording. Before each recording, bile aliquots were diluted 1:1000 in water from the EOG system. There were no significant differences in olfactory responses between males and females, hence responses of both sexes were averaged together. The percentage reduction in olfactory activity was calculated by dividing the amplitude of the olfactory signal at time $\times$ (mV) by amplitude of the olfactory signal at time 0 (mV) * 100. Percentage of olfactory signal reduction between control and treated naris was calculated as follows (Amplitude response to odorant in control naris (mV) - Amplitude response to odorant in treated naris (mV))/Amplitude response to odorant in control naris (mV)) * 100.

2.7. Behavioral assays

Two-choice maze behavioral assays (Buchinger et al., 2017) were used to evaluate zebrafish responses to food odors pre and post exposure to treatments at 3 h (time of losing olfactory sensitivity in EOGs) and 3 d exposure (time of recovery of olfactory sensitivity in EOGs). An experimental two-choice maze was constructed using acrylic sheets with a submersible water pump (PondmasterTM POND MAG3) to create inflow, and a multichannel peristaltic pump to release food odor (Cole-Parmer® CatalystTM Masterflex FH Series) in one channel and deionized water in the other channel. A meshed barrier was added to create a laminar flow dispersed the cue evenly through the odor channel (Jutfelt et al., 2017).

Behavior trials were conducted on adult zebrafish (N = 8). Food was withheld for 24 h prior to trials. Zebrafish were lightly anesthetized using 0.2 g/L MS222 (Sigma Aldrich). Fish nares were flushed with 3 μl of recombinant SARS-CoV-2 S RBD protein (50 ng/μl) in PBS, an unrelated His-tagged recombinant protein (Sepahi et al., 2017) from here on termed r-CK12a (3 μl at 50 ng/μl) in PBS or PBS alone. Fish were returned to their tanks to recover for 3 h or 3 d prior to the behavior experiment. The behavioral trials had four phases, acclimation (10 min) in a holding chamber, exploration (10 min), re-acclimation (10 min), and exposure to food cue (10 min). The time zebrafish spent in each side was recorded in seconds. For the trial to be considered successful, zebrafish had to explore both chambers. Side preference was determined during initial exploration phase and food odor was released to the opposite side during cue trials. Food cue was 1 g of Tetra® TetraFin Goldfish Flake food homogenized in 1L of deionized water. The odor was created 24 h before experiments and was stored at 4 °C until the trials, when it was brought to room temperature. Control cue was deionized water for all trials.

During trials the time spent in the control and experimental channels were recorded and an index of preference (i) was calculated for each test (i = [ae/(ae + be) – ac/(ac + bc)]). The time spent in the control channel before odor exposure was calculate (bc = before odor release control channel and be = before odor release experimental channel, respectively), and after odor exposure (ac = after odor release control channel and ae = after odor release experimental channel). The indices of preference range between 1 (positive preference or attraction) and −1 (negative preference or repulsion), index of preference 0 indicates that fish have no preference for spending time in either channel.

2.7.1. Statistical analysis

All data were checked for normal distribution prior to performing statistical analyses using F test or Bartlett's. Unpaired t-tests or one-way ANOVA followed by a Tukey's post hoc comparison were used to detect differences among treatments in all histological and IF staining studies. For scRNA-Seq population proportion analysis of number of cells in each cluster across treatments we used R (v1.2.5001) with prop.test and P-values were adjusted using p.adjust set to the "bonferroni" method. For behavioral tests, a Wilcoxon matched pairs signed-rank test ($\alpha = 0.05$) was used to evaluate differences from significant preference (swimming towards or against the food cue) or no preference at all for the food odor (random swimming) in each treatment. Statistics were done in GraphPad Prism V7.0d. P-values were as follows: * P-value < 0.05, ** P-value < 0.01, *** P-value < 0.001, and **** P-value < 0.0001.

2.8. Data and code availability

The fastqs generated for the scRNA-Seq of this study are available on NCBI under the Bioproject PRJNA668529.

3. Results

3.1. Comparative analyses of ACE2 molecules in vertebrates

The ACE2 protein is the receptor for SARS-CoV-2 S RBD on permissive human cells and expressed in the sustentacular cells of the mammalian OE (Brann et al., 2020; Hoffmann et al., 2020b). Comparative analysis of angiotensin-converting enzyme 2 (ACE2) molecules in vertebrates indicated a 72%-73% similarity and 57.5%-58% identity between zebrafish Ace2 and human ACE2, respectively (Table S1). Examination of ACE2 amino acids in the region involved in binding SARS-CoV-2 S protein (Liu et al., 2020) revealed modest conservation of amino acids in zebrafish Ace2 at the binding interface (Table S2). Combined, these data agree with previous reports and suggest that teleost ACE2 proteins are not likely to bind SARS-CoV-2 S (Damas et al., 2020).

3.2. Intranasal delivery of SARS-CoV-2 S RBD causes olfactory damage in adult zebrafish

Anosmia is one of the earliest manifestations of SARS-CoV-2 infection in humans (Cooper et al., 2020). We have previously shown that IHNV glycoprotein is sufficient to induce rapid nasal immune responses as well as neuronal activation in teleost fish (Sepahi et al., 2019). Thus, we hypothesized that recombinant SARS-CoV-2 S RBD protein may be sufficient to damage the OO of zebrafish. In order to test this hypothesis, we delivered recombinant SARS-CoV-2 S RDB to the nasal cavity of adult AB zebrafish and sampled the OO 3 h (h), 1 day (d), 3 d, 5 d and 2 weeks (w) later. Negative controls consisted of animals that received vehicle only (PBS) into the nasal cavity as well as fish that received the same dose of r-CK12a. We also included a Poly(I:C) treated group as an additional control for dsRNA induced antiviral effects. SARS-CoV-2 S RBD was sufficient to cause severe damage to the zebrafish OO at all early time points examined (Fig. 1A-E). Tissue damage was characterized by presence of edema and endothelial inflammation in the lamina propria as early as 3 h post-treatment (Fig. 1A-B & J). Presence of
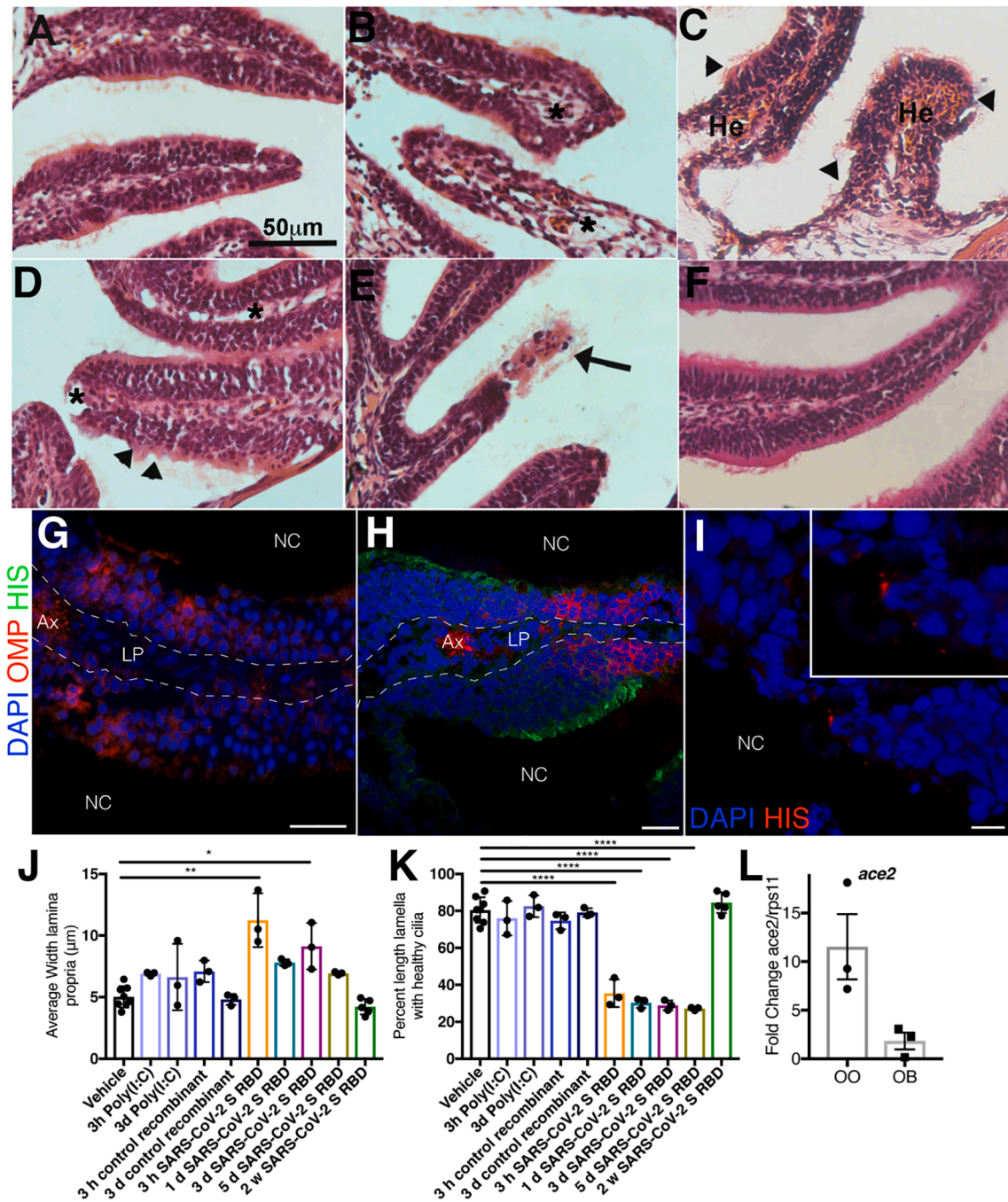
Fig. 1. Intranasal delivery of SARS-CoV-2 S RDB protein causes severe histological damage in the adult zebrafish OO that recovers after 2 weeks. H&E stains of zebrafish OO paraffin sections. (A) Control vehicle treated OO. (B) 3 h; (C) 1 d; (D) 3 d; (E) 5 d; (F) 2 w post intranasal delivery of SARS-CoV-2 S RDB protein (r-Spike) or controls (Poly(I:C) and an off-target His-tagged recombinant protein). Images are representative of n = 10 sections per animal and *N* = 3–5 fish per experimental group. Asterisk denotes edemic spaces in the olfactory lamellae, mostly in the lamina propria. He: hemorrhages. Arrow heads: apical loss of olfactory sensory neurons. Black Arrow: Necrotic lamella. (G) Immunofluorescence image of an AB zebrafish OO cryosection from an adult OMP:lynRFP animal 15 min after I.N SARS-CoV-2 S RBD administration stained with a rabbit IgG isotype control as primary antibody. Scale: 20 µm. (H) Immunofluorescence image of an OMP:lynRFP zebrafish OO stained with anti-His antibody (green) 15 min post I.N. delivery of recombinant His-tagged SARS-CoV-2 S RBD. (I) Immunofluorescence of an AB zebrafish OO stained with anti-His antibody (red) 15 min post I.N. delivery of SARS-CoV-2 S RBD shows puncta of anti-His staining when zoomed in on non-sensory epithelium; Scale = 5 µm. Ax: OSN axon bundles; NC: nasal cavity; LP: lamina propria. Scale: 20 µm. Cell nuclei are stained with DAPI (blue). (J) Mean width of the olfactory lamina propria in each treatment group. (K) Mean percent of olfactory lamellar surface covered by healthy cilia in each treatment group. (L) Expression of *ace2* in OO and OB tissue of untreated adult AB zebrafish (*N* = 3) as measured by RT-qPCR. Expression levels were normalized to *rps11* as the house-keeping gene. Quantifications in J&K were performed in ImageJ; error bars represent S.E.M. J&K statistics were done by one-way ANOVA followed by a Tukey's post hoc comparison. * *P*-value < 0.05, ** *P*-value < 0.01, **** *P*-value < 0.0001.

hemorrhages at the tip and base of the olfactory lamellae was observed 1 d post-treatment (Fig. 1C). Edema, characterized by empty spaces in the tissue (asterisks in Fig. 1), was observed in the epithelium at 3 h, but by 1 d, 3 d, and 5 d edemic spaces were found throughout the lamina propria. Further, we quantified edema by measuring the width of lamina propria at 50 μm from the raphe and found significant expansion of the lamina propria at 3 h and 3 d after I.N SARS-CoV-2 S RBD delivery (Fig. 1J). Loss of the epithelial mosaic structure characteristic of the teleost olfactory epithelium (Byrd and Brunjes, 1995) was observed 1 d, 3 d and 5 d post-treatment (Fig. 1C-E). By 5 d, loss of entire lamella due to severe necrosis was observed in the SARS-CoV-2 S RBD treated animals, whereas no control animals lost lamellae (N = 3) (Fig. 1E). Significant loss of olfactory cilia was recorded in all animals treated with SARS-CoV-2 S RBD at all early time points (Fig. 1K). Specifically, all animals treated I.N. with SARS-CoV-2 S RBD had areas along the olfactory lamellae where cilia were tangled in dense knots, sheared to less than 1 μm or completely detached. No olfactory damage was observed in zebrafish that received r-CK12a or Poly(I:C) (Fig. 1J-K, Figure S1 & S2). To evaluate the recovery of the OO after I.N. delivery of SARS-CoV-2 S RBD, we examined histological sections 2 w post-treatment. Studies into the plasticity of the zebrafish olfactory system show that by 2 w after chemical ablation of the OO, structure and function are restored (Calvo-Ochoa and Byrd-Jacobs, 2019). By 2 w after I.N. SARS-CoV-2 S RBD the OO resembled the vehicle treated OO (Fig. 1F). The mosaic of the neuroepithelium was restored; there was no edema and the cilia appeared healthy (Fig. 1F & J-K). These results indicate that SARS-CoV-2 S RBD is sufficient to cause severe but transient tissue damage in the zebrafish OO and that olfactory damage can occur in the absence of active SARS-CoV-2 replication.

To localize interactions between the recombinant SARS-CoV-2 S RBD protein and the OO, we performed immunofluorescence staining with an anti-His antibody 15 min after SARS-CoV-2 S RBD recombinant protein treatment in OMP:lynRFP animals that endogenously express red fluorescent protein (RFP) in mature ciliated OSNs (Sato et al., 2005). SARS-CoV-2 S RBD protein was widely localized along the non-sensory epithelium, as evidenced by the lack of RFP signal in anti-His positive regions (Fig. 1H). Additionally, a magnified view of the non-sensory area of a wild type zebrafish OO 15 min after being treated I.N. with SARS-CoV-2 S RBD shows limited, punctate anti-His staining pattern along the non-sensory epithelial area of the lamellae (Fig. 1I). Both the isotype control stain on 15 min SARS-CoV-2 S RBD treated animals and anti-His stain on vehicle treated animals showed no signal in these areas (Fig. 1G & S3).

To assess whether the zebrafish homolog *ace2* is expressed in the olfactory system of zebrafish we measured transcript levels by qPCR on the OO and OB of control adult zebrafish (Fig. 1L). We confirmed moderate expression levels of *ace*2 in the zebrafish OO but very low levels in the OB. Therefore, it is possible that the SARS-CoV-2 S RBD is interacting with Ace2 in the zebrafish OO although other mechanisms of ligand-receptor interaction cannot be ruled out.

3.3. Intranasal SARS-CoV-2 S RBD delivery alters the OO lamina propria in adult zebrafish

Based on H&E analysis, large fibrous patches are evident in the lamina propria of the zebrafish OO 3 d post I.N. SARS-CoV-2 S RBD delivery (Fig. 2A). Lung tissue fibrosis is a hallmark in SARS-CoV-2 and SARS-CoV patients (Beigmohammadi et al., 2020; Tian et al., 2020; Xu et al., 2020; Zuo et al., 2010) characterized by fibroblast persistence and excessive deposition of collagen and other extracellular matrix components (Zuo et al., 2010). To determine if the changes observed in the zebrafish OO lamina propria could be similar to those found in lung fibrosis, we performed Masson Trichrome stains which stain collagen blue. Compared with the control (Fig. 2B) there was no increase of blue stained collagen deposits at 3 h (Fig. 2C-D) or 3 d (Fig. 2E-F) in SARS-CoV-2 S RBD animals. However, by 3 d large amounts of bright red deposits were observed suggesting that the fibrous material present in

the lamina propria of treated animals is composed of keratins and may contribute to tissue healing (Fig. 2F) (Paladini et al., 1996). Although not previously used in zebrafish OO studies, cytokeratin 8 (CTK8) is an epidermal marker during regeneration in zebrafish (Martorana et al., 2001). CTK8 staining in control adult zebrafish OO revealed positive staining pattern in the non-sensory epithelium as well as in SCs and basal cells (Fig. 2G & S7A). I.N. Poly(I:C) treatment did not alter the CTK8 staining pattern in the OO (Figure S4A-B). At 3 h after I.N. SARS-CoV-2 S RBD treatment the mosaic of the non-sensory epithelium was disrupted; the usually flat morphology of the progenitor horizonal basal cells became rounded and the columnar SCs were less evident (Fig. 2H & S7B). By 3 d after SARS-CoV-2 S RBD the non-sensory epithelium was highly disorganized, and the CTK8 staining was localized in some cells of the lamina propria, in sharp contrast with control or 3 h OO samples where the lamina propria was CTK8 negative (Fig. 2G-I & S7A-C).

We were curious if this change in CTK8 immunoreactivity pattern may be due to changing cellular dynamics of the OO in response to damage to the lamina propria and OE (Fig. 1 & 2C-F). Therefore, we used an anti-PCNA antibody to assess cells in the synthesis phase of cell division. OO cryosections stained with an isotype control instead of anti-PCNA antibody showed no antibody reactivity (Figure S5A). Compared to vehicle treated OO, there was a significant increase in the number of cells positive for PCNA reactivity at 3 h (Fig. 2J-K) and 3 d (Fig. 2J-L) after I.N. SARS-CoV-2 S RBD (Fig. 2Q). Similar to past studies in the zebrafish OO, most PCNA positive cells were located in the non-sensory epithelium, although some were in the sensory region of the lamella (Figure S7D-F) (Bettini et al., 2016). Importantly, the number of PCNA positive cells at 3 d after I.N. SARS-CoV-2 S RBD was different than at 3 d after delivery of the viral mimic Poly(I:C), echoing the histological differences observed between the two treatment groups (Fig. 2Q & S4C-D). Further, due to the loss of OSN cilia (Fig. 1K) we were curious if cells within the neuroepithelium were apoptotic. Therefore, we stained OO cryosections with an anti-activated caspase-3 antibody and counted positive cells as those with bleb-shaped apoptotic bodies. OO cryosections stained with an isotype control instead of anti-activated caspase-3 antibody showed no antibody reactivity (Figure S5B). We found a significant increase in apoptotic cells after 3 h and 3 d I.N. SARS-CoV-2 S RBD (Fig. 2M-P & S7G-I) mostly located in the non-sensory epithelium at 3 h and 3 d and some clusters of cells present in the sensory epithelium by 3 d. Multiple Poly(I:C) I.N. deliveries are known to induce apoptosis in the mouse OO (Kanaya et al., 2014), whereas a single delivery of Poly (I:C) I.N. caused apoptosis in the rainbow trout OO 4 h post-treatment (Sepahi et al., 2019). In the present study, a single I.N dose of viral mimic Poly(I:C) did not cause significant apoptosis compared to previous findings in rainbow trout, however the triple Poly I:C treatment did (Figure S6B and D). Due to this discrepancy, we also employed the known olfactotoxic drug methimazole (Chen et al., 2017; Leung et al., 2007; Suzukawa et al., 2011) and found significantly higher numbers of activated caspase 3^+ compared to the triple Poly(I:C) treatment (Figure S6C-D). Importantly, apoptosis 3 d after I.N. SARS-CoV-2 S RBD delivery mostly occurred in the non-sensory regions (Figure S7I) corresponding to the area of high anti-His 6x immunoreactivity (Fig. 1H). Together, our data indicate that I.N. delivery of SARS-CoV-2 S RBD causes dynamic changes in the zebrafish OO supporting cells and the lamina propria, where OSN axon bundles, *fila olfactoria*, are located. The observed changes may correspond to wound repair responses in the lamina propria resulting from SARS-CoV-2 S RBD induced damage.

3.4. Intranasal delivery of SARS-CoV-2 S RBD causes anosmia but does not alter behavioral preference for food in adult zebrafish

We were curious to investigate whether histological findings translated into functional changes to the OO. Adult zebrafish given SARS-CoV-2 S RBD I.N. had an instant, significant reduction of olfactory response to food extracts with a 50% reduction in amplitude on electro-olfactogram recordings (EOG) compared to pretreatment response to
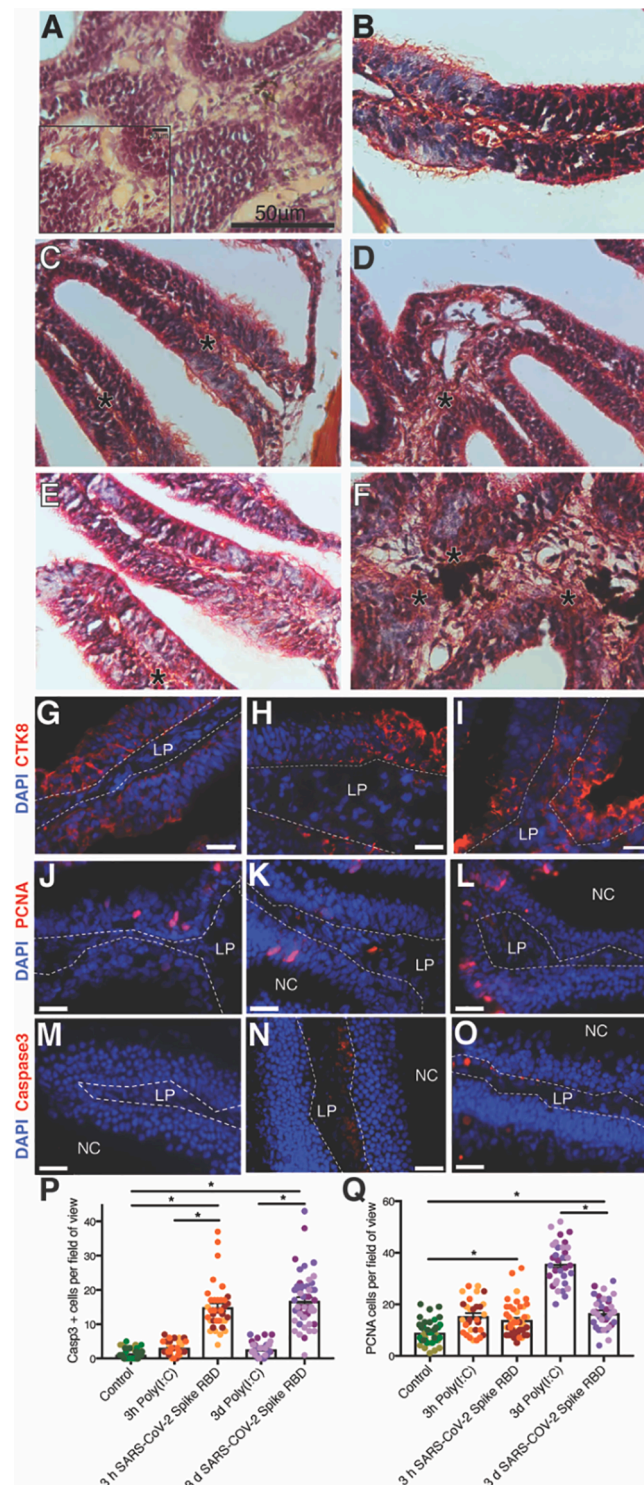
Fig. 2. Intranasal delivery of SARS-CoV-2 S RDB protein causes severe cellular changes to the OO of adult zebrafish. (A) H&E image of raphe of the OO showing large eosinophilic deposits 3 d post intranasal delivery of SARS-CoV-2 S RBD (B) Masson Trichrome stains of zebrafish OO administered intranasally vehicle or (C-D) 3 h SARS-CoV-2 S RBD, or (E-F) 3 d SARS-CoV-2 S RBD. Asterisk denotes red keratin deposits. Blue staining corresponds to collagen deposits. (G) anti-CTK8 (red) immunofluorescence staining of adult zebrafish OO cryosections after intranasal delivery of vehicle or (H) 3 h; or (I) 3 d SARS-CoV-2 S. (J) anti-PCNA immunofluorescence staining of adult zebrafish OO cryosection after intranasal delivery of vehicle or (K) 3 h; or (L) 3 d recombinant SARS-CoV-2 S RBD. (M) anti-caspase3 (red) immunofluorescence staining of adult zebrafish OO cryosections after intranasal delivery of vehicle or (N) 3 h; (O) 3 d recombinant SARS-CoV-2 S RBD. Nuclei are stained with DAPI (blue). Scale in (G-O): 20 μm. (P) Quantification of the mean number of caspase3 positive cells per field of view. (Q) Quantification of number of PCNA positive cells per field of view. Quantifications shown in P and Q were performed on $N = 4$ animals and n = 10 fields of view per animal, represented by different colors. Error bars represent S.E.M. LP: lamina propria; NC: nasal cavity. Statistics ANOVA followed by a Tukey's post hoc comparison. *P-value < 0.05. Representative images of Poly(I:C)-treated animals are shown in Supplemental Fig. 2.
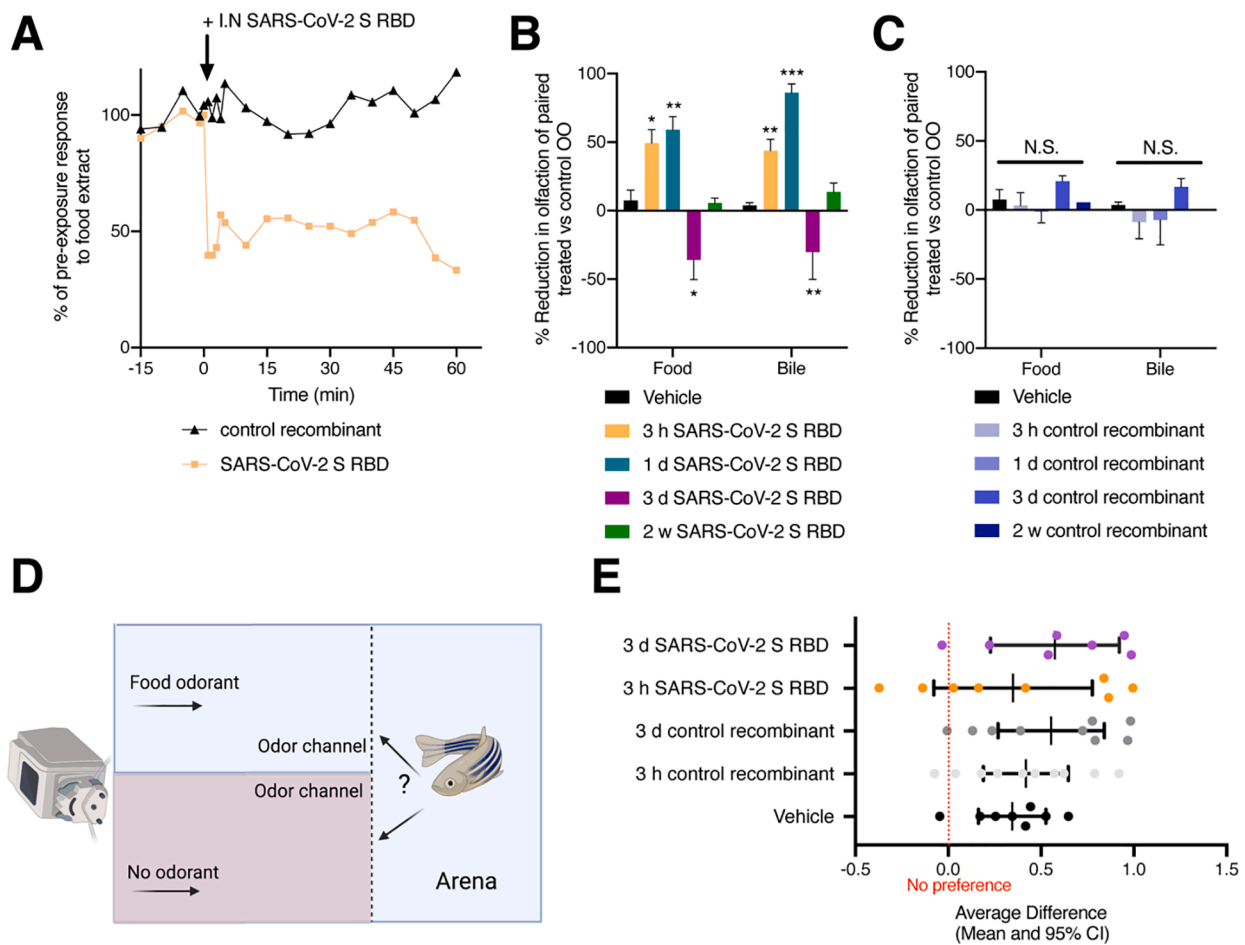
Fig. 3. Intranasal delivery of SARS-CoV-2 S RDB protein causes anosmia in adult zebrafish. (A) Representative EOG of adult zebrafish showing olfactory responses to food over time before and after addition of SARS-CoV-2 S RDB protein (yellow) or a control recombinant protein (black) to the naris normalized to pre-exposure values. (B) Mean percentage loss of olfactory detection of food or bile salts measured by EOG recording. Adult zebrafish ($N = 4$) were treated with SARS-CoV-2 S RDB protein in one naris or vehicle control (PBS) in the other naris for 3 h (yellow), 1 d (teal), 3 d (purple) or 2 w (green) after which EOG were recorded by exposing animals to either food odorant or bile and recording electrical responses in each individual naris. The percent reduction was calculated as percent of the SARS-CoV-2 S RDB treated naris EOG response to vehicle treated naris EOG response. (C) Mean percentage loss of olfactory detection of food or bile salts measured by EOG recording. Adult zebrafish ($N = 4$) were treated with control recombinant protein (r-CK12a) in one naris or vehicle control (PBS) in the other naris for 3 h, 1 d, 3 d or 2 w after which EOG were recorded by exposing animals to either food or bile and recording electrical responses in each individual naris. The percent reduction was calculated as percent of the control recombinant treated naris EOG response to vehicle treated naris EOG response. (D) Graphical representation of the behavioral choice test used in this study. (E) Calculated average difference in time spent on the half of arena containing food odorant or on the half of the arena containing vehicle odorant after adult zebrafish were treated I.N. with vehicle, 3 h or 3 d SARS-CoV-2, or 3 h or 3 d control recombinant (r-CK12a). Red dotted line represents average difference if fish displays zero preference for either odor. Statistical analyses for (B & C) were determined by ANOVA with Tukey's post hoc multiple comparison whereas a Wilcoxon match pairs signed-rank test was used for behavioral analysis in (E). Error bars in B & C represent S.E.M. and error bars in E represent 95% confidence interval (CI). * *P*-value < 0.05; ** *P*-value < 0.01; *** *P*-value < 0.001.

food odor (Fig. 3A & S8). Reduction in the olfactory response was detected within 1 min of exposure to SARS-CoV-2 S RBD, indicating an instant change in olfactory function (Fig. 3A). The olfactory responses to the food odorant were recorded for 4 sec every 5 min for total period of 1 h. During the 5 min resting periods, OO was flushed with water to clean excess odorant and avoid desensitization of the OSN by overexposure. Reduction of olfactory responses to food extract in SARS-CoV-2 S RBD treated fish was sustained for 1 h. We repeated the same sequential exposure to food odors in individuals treated with PBS and responses to food odorant were not reduced at any time point in these control treatments (Fig. 3A). This confirmed that reduction of olfactory responses to food extracts in SARS-CoV-2 S RBD treated individuals was not due to desensitization of the OSN by overexposure to food odorant but related to a damage to the OO. To further quantify the degree of olfactory reduction due to I.N. SARS-CoV-2 S RBD, we took advantage of the two separate olfactory chambers present in zebrafish. We exposed one naris to the SARS-CoV-2 S RBD protein and the other naris, in the

same animal, to vehicle (PBS) and waited 3 h, 1 d, 3 d or 2 w before measuring olfaction by EOG (Fig. 3B). At 3 h, we observed the SARS-CoV-2 S RBD naris had a 49% and 44% reduction in olfactory responses to food and bile, respectively, compared to the vehicle treated naris and a 60 and 89% loss of olfactory function in food and bile olfactory responses respectively 1 d post-treatment (Fig. 3B). Some individuals showed no EOG responses for bile in the treated naris with SARS-CoV-2 S RBD after 1 d. The reduction in olfactory sensitivity to food extract was smaller than that found for bile, probably due to the lower number of OSNs involved in bile acid detection compared to amino acids found in food (Hansen et al., 2003). At 3 d, EOG responses for food and bile of the SARS-CoV-2 S RBD treated naris were slightly higher than and vehicle treated naris (shown as negative value of reduction in Fig. 3B), indicating an overcompensation of the treated naris which is therefore more sensitive to food and bile odors. After 2 w post I.N. SARS-CoV-2 S RBD treatment, EOG responses between nares were not different (Fig. 3B). EOG responses to food and bile 3 h, 1 d, 3

d and 2 w after I.N. a control recombinant protein (r-CK12a) were not significantly different from the vehicle treated naris (Fig. 3C). Our results indicate that EOG observed SARS-CoV-2 S RBD-induced-anosmia is not specific for a subset of OSNs, since both food extracts and bile olfactory signals were suppressed in SARS-CoV-2 S RBD treated zebrafish.

To learn if exposure to SARS-CoV-2 S RBD altered behavior of adult zebrafish due to olfactory dysfunction, we performed a two-choice maze decision test, where fish could swim into a maze with two water channels, one with continuous release of a food odor and the other releasing water (Fig. 3D). A positive index preference demonstrates a behavior
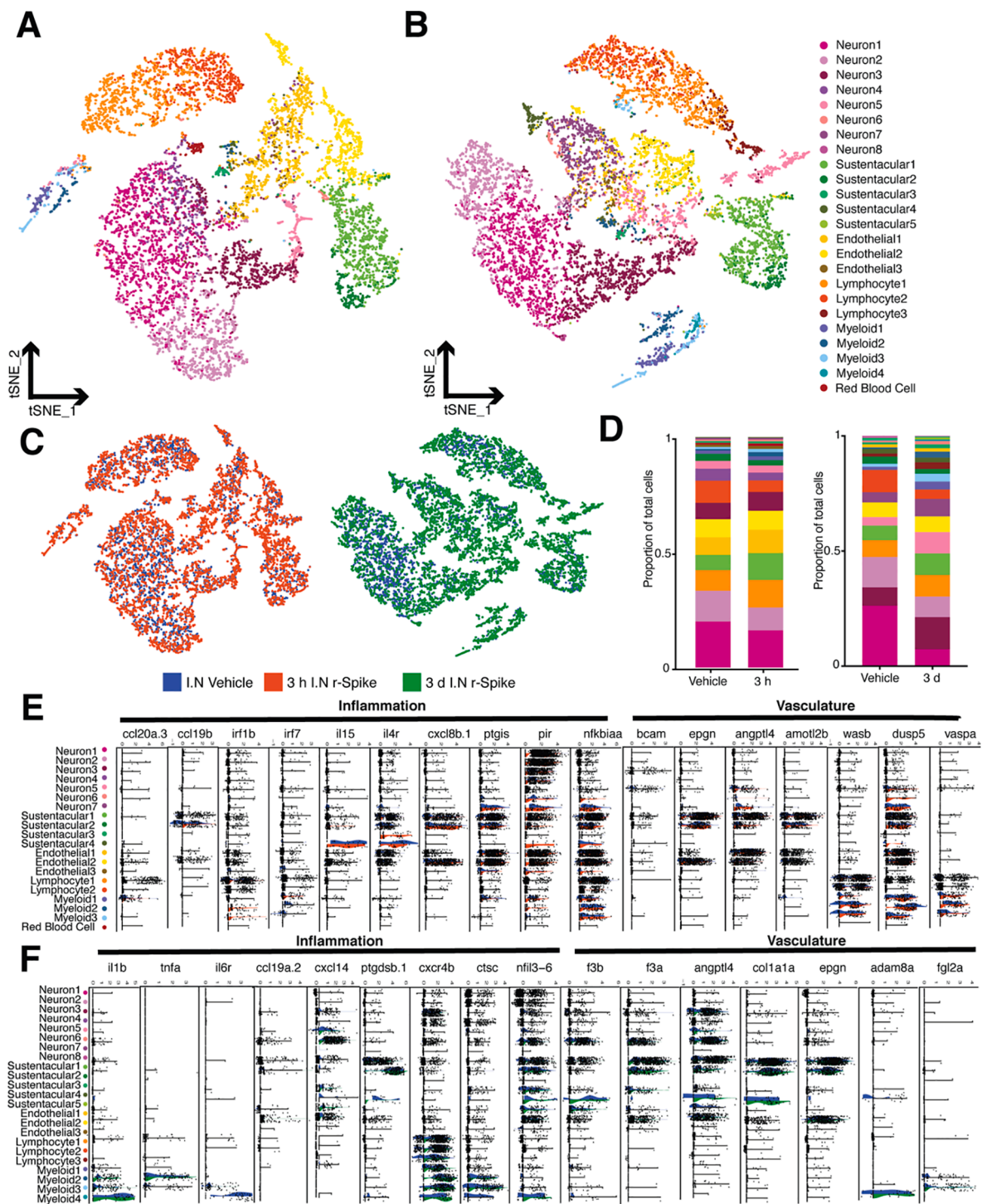

Fig. 4. ScRNA-Seq of zebrafish OO reveals changes in cellular landscape due to intranasal SARS-CoV-2 S RBD protein delivery. (A-B) Cellular composition of the zebrafish OO visualized using t-distributed stochastic neighbor embedding (tSNE) of vehicle treated, 3 h and 3 d post-intranasal delivery of SARS-CoV-2 S RBD (r-Spike). Individual single-cell transcriptomes were colored according to cluster identity. tSNE plots were generated in Seurat and identified 20 and 22 distinct cell clusters, respectively. (C) tSNE plots of zebrafish OO cell suspensions colored according to treatment. (D) Bar plots showing the proportion of cells belonging to each cluster in each treatment group. Statistical analysis for changes in cell population proportions is in supplemental tables 3 and 4. (E-F) Violin plots showing expression of selected markers of inflammation and vasculature remodeling in the 3 h SARS-CoV-2 S RBD (orange) versus vehicle treated (blue) and 3 d SARS-CoV-2 S RBD (green) versus vehicle treated (blue) zebrafish OO obtained by scRNA-Seq. All represented genes were significantly differentially regulated between treatments (adjusted *P*-value-adj < 0.05).

towards choosing the food odor, while a negative index preference shows behavior choosing no odor. An index of preference of 0 means that fish are swimming randomly between the two channels (indicated by the red dotted line in Fig. 3E). Animals given vehicle (PBS) I.N. spent more time swimming in the channel with the food cue, as indicated by the positive index of preference that was significantly different from index of preference 0 (Fig. 3E). Animals given vehicle (PBS) or r-CK12a I.N. swam more during the test compared to animals given SARS-CoV-2 S RBD I.N. (data not shown). After r-CK12a I.N. animals displayed preference to food similar to what we observed in vehicle treated animals (Wilcoxon match pairs signed rank test p = 0.641 at 3 h and p = 0.297 and 3 d). Comparisons between 3 h and 3 d CK12a I.N. treated animals did not find any differences between treatments (Wilcoxon match pairs signed rank test p = 0.36) (Fig. 3E). Furthermore, there was no significant difference in preference to the food odor between SARS-CoV-2 S RBD treated groups and respective vehicle controls at any examined time point (p = 1 at 3 h; p = 0.469 at 3 d). Comparison between zebrafish 3 h I.N. SARS-CoV-2 S RBD and 3 d 3 h I.N. SARS-CoV-2 S RBD also did not show any statistically significant difference (p = 0.58) (Fig. 3E). Thus, altered EOG responses in SARS-CoV-2 S RBD treated zebrafish were not paralleled by behavioral changes in food preference at least in our behavioral paradigm.

3.5. Single-cell analysis of the zebrafish olfactory organ

To better understand the mechanisms of SARS-CoV-2 S RBD induced olfactory dysfunction in adult zebrafish, we performed single cell RNA-Seq (scRNA-Seq). Given our histological findings and binding of the SARS-CoV-2 S RBD to the non-sensory epithelial region, we hypothesized that transcriptional perturbations occur in sustentacular cells as well as in OSNs due to indirect mechanisms. scRNA-Seq was performed after 3 h or 3 d of I.N. administration with SARS-CoV-2 S RBD. These timepoints were selected based on the histological findings of Fig. 1. Data from the treated time point was integrated with that from vehicle treated controls in Seurat and then clustered using 30 significant principal components (Fig. 4A-B) (Butler et al., 2018). We identified a total of 8 neuronal cell clusters (NC), 5 SC clusters, 3 endothelial cell (EC) clusters and 7 leucocyte (lymphoid and myeloid) clusters (Fig. 4A-B).

Of the 8 NCs, Neuron1 and Neuron2 corresponded to mature OSNs. Neuron1 expressed markers of ciliated OSNs (*ompa* and *ompb*) in addition to several olfactory receptor (OR) genes (Buiakova et al., 1996). Neuron2, on the other hand, expressed markers of microvillus OSNs (*trpc2b, s100z,* and *gnao*) and many VRs such as *v2rh32* as well as OR genes (Figure S9) (Kraemer et al., 2008). Neuronal clusters 3–8 included OSNs in different differentiation stages, from progenitor-like neurons to differentiating intermediate neuronal precursors (Yu and Wu, 2017). For instance, expression of multiple high mobility group transcripts (*hmga1a,* and *hmgb2b2*) typically found in neuronal precursor cells is expressed inversely to the transcription factor family of sox genes (*sox4* and *sox11*) associated with committing to differentiation to mature neurons across the neuronal subsets (Bergsland et al., 2006; Giancotti et al., 2018). The Neuron3 cluster expressed both *ompa* and OR genes as well as markers of neuronal differentiation and plasticity such as *neurod1, neurod4, gap43, sox11*, and *sox4* suggesting commitment to becoming mature ciliated OSNs. The cluster Neuron4, only found at 3 h, was transcriptionally similar to the Neuron3 cluster expressing *hmga1a,* and *hmgb2b2*, but lacked markers of differentiation (*gap43* and *sox11*) indicating a state closer to a neuronal progenitor. The clusters Neuron5 and Neuron6 were the closest to the progenitor state with expression of basic helix-loop-helix transcription factors (i.e. *bhlhe23*), associated with exit from the cell cycle and progenitor state, as well as cell cycle genes (Borders et al., 2007). Clusters Neuron7 and Neuron8 expressed cell cycle and early neuronal progenitor markers as well as *tmprss13b* and *tmprss4a,* however the majority of cluster identifying genes in these two clusters are undescribed (Figure S9).

SCs are supporting cells that exist in the neuroepithelium around

OSNs and in humans, they express ACE2 (Sungnak et al., 2020). SCs in the OE can directly arise from horizontal basal cells (HBCs) (Yu and Wu, 2017). We found 5 clusters of SCs in our datasets. Sustentacular clusters 1 and 2 had similar expressing markers to those of HBCs (*krt5*) and other basal cells (*lamc2* and *col1a1b*) and therefore may represent olfactory basal cells (Chen et al., 2017; Peterson et al., 2019). Further, these clusters expressed immune genes such as *ptgs* and *ccl25*, and HBCs are known to express immune factors in models of olfactory epithelium damage (Chen et al., 2019). Interestingly, in addition to *sox2* expression, Sustentacular3 cluster expressed *atoh1,* a basic helix loop helix gene important in hair cell regeneration (Bermingham-McDonogh and Reh, 2011). Cluster Sustentacular4 expressed cytokines *il15* and *il17a/f3* as well as *ace*. The last SC cluster was only found in the 3d time point and markers suggest it is a subpopulation closely related to the Sustentacular4 cluster (Figure S9).

We identified three clusters of ECs that all express *tmprss13* and *tmprss4*. Unfortunately, while using *ace2* specific primers in RT-qPCR detected expression in both the OO and OB (Fig. 1L), *ace2* expression was detected in only a few cells of our scRNA-Seq dataset (not shown). This may be due to the cell isolation protocol used in our study. Furthermore, low *ace2* expression levels in neuronal tissues as well as in our tissue samples may be hard to detect by high throughput scRNA-Seq which is known to have gaps in transcriptional coverage when capturing thousands of cells (Figure S9) (Song et al., 2021). Endothelial1 and 2 clusters expressed the endothelial markers *sox7* and *tmp4a* (Yao et al., 2019). All three clusters broadly expressed genes associated with tight junctions (*tjp3, jupa, ppl, cldne,* and *cgnl1*) as well as many keratin genes (Figure S9). Interestingly, Endothelial3 cluster also expressed the calcium channel *trpv6* and a slew of non-annotated genes.

There are copious amounts of immune cells in the teleost OO (Mellert et al., 1992; Tacchi et al., 2014), and although our method of generating single cell suspensions for scRNA-Seq was optimized for neuronal cell viability, we captured small groups of both myeloid and lymphoid cells in our samples. Lymphocyte1 cells expressed classical T cell markers (*cd8, cd4,* and *zap70*) as well as *ccr9,* a mucosal homing chemokine receptor, and novel immune type receptor genes (*nitrs*) thought to be natural killer cell receptors (Papadakis et al., 2003; Wei et al., 2007). Therefore, we propose that lymphocyte1 are a type of innate-like NKT cells. Lymphocyte2 cluster cells expressed the transcription factor *foxp3b* found in regulatory T cells (T$_{regs}$). The 3 d time point revealed a third lymphocyte cluster with classical T cell identity. The myeloid cell clusters 1–3 expressed MHC II complex genes as well as *mpeg1.1,* a marker of zebrafish macrophages (Ellett et al., 2011). Myeloid4 cluster expressed *mpx,* a marker for neutrophils, and no antigen presentation genes (Yoo and Huttenlocher, 2011). Each macrophage-like myeloid cluster expressed unique cytokines contributing to their separate clustering - Myeloid1 expressed *il12* and *il22,* Myeloid2 expressed *il1fma* and *il10ra,* and Myeloid3 expressed *il6r* and *il1b*. Together, these data indicate that the zebrafish OO is a heterogeneous neuroepithelium with diverse immune cell subsets.

3.6. Intranasal delivery of SARS-CoV-2 S RBD induces inflammatory responses and widespread loss of olfactory receptor expression in adult zebrafish olfactory organ

Given the changes in morphology viewed from histology and cellular dynamics as well as the altered EOG responses to odorants, we hypothesized that SARS-CoV-2 S RBD treatment caused transcriptomic changes in OSNs. The cellular landscape of the zebrafish OO was affected by SARS-CoV-2 S RBD treatment and time (Fig. 4A-D). This was especially evident in the proportions of neuronal cell types 3 d post-treatment when the proportion of mature, *omp* expressing ciliated OSN was significantly lower compared to controls and the 3 h treated group (Tables S3 & S4). In contrast, neuronal progenitors expressing cell cycle markers (*aubk, ecrg4,* and *mki67*) and neuronal differentiation and plasticity markers (*neurod1, neurod4, gap43, sox11*, and *sox4*) were

expanded 3 d post-treatment (Fig. 4B-C & Table S4). Interestingly, many of these plasticity associated genes were found in a greater number of single nuclei transcriptomes collected from post mortem human parenchyma in COVID-19 and Influenza A patients than control (Yang et al., 2021). Further, we detected a significant decrease in the proportion of cells belonging to the Lymphocyte2 cluster, a cluster that expressed

markers of T_{reg} cells (*foxp3b*) 3 h post I.N. delivery of recombinant SARS-CoV-2 S RBD (Fig. 4C & Table S3). At 3 d, we observed a third lymphocyte cluster, not detected at 3 h, highly expressing the TCR subunit *zap70* as well as plac8 onzin related protein (*ponzr1*), a molecule that has immunoregulatory roles during Th1 type immune responses in mammals (Figure S9) (Slade et al., 2020). These results indicate
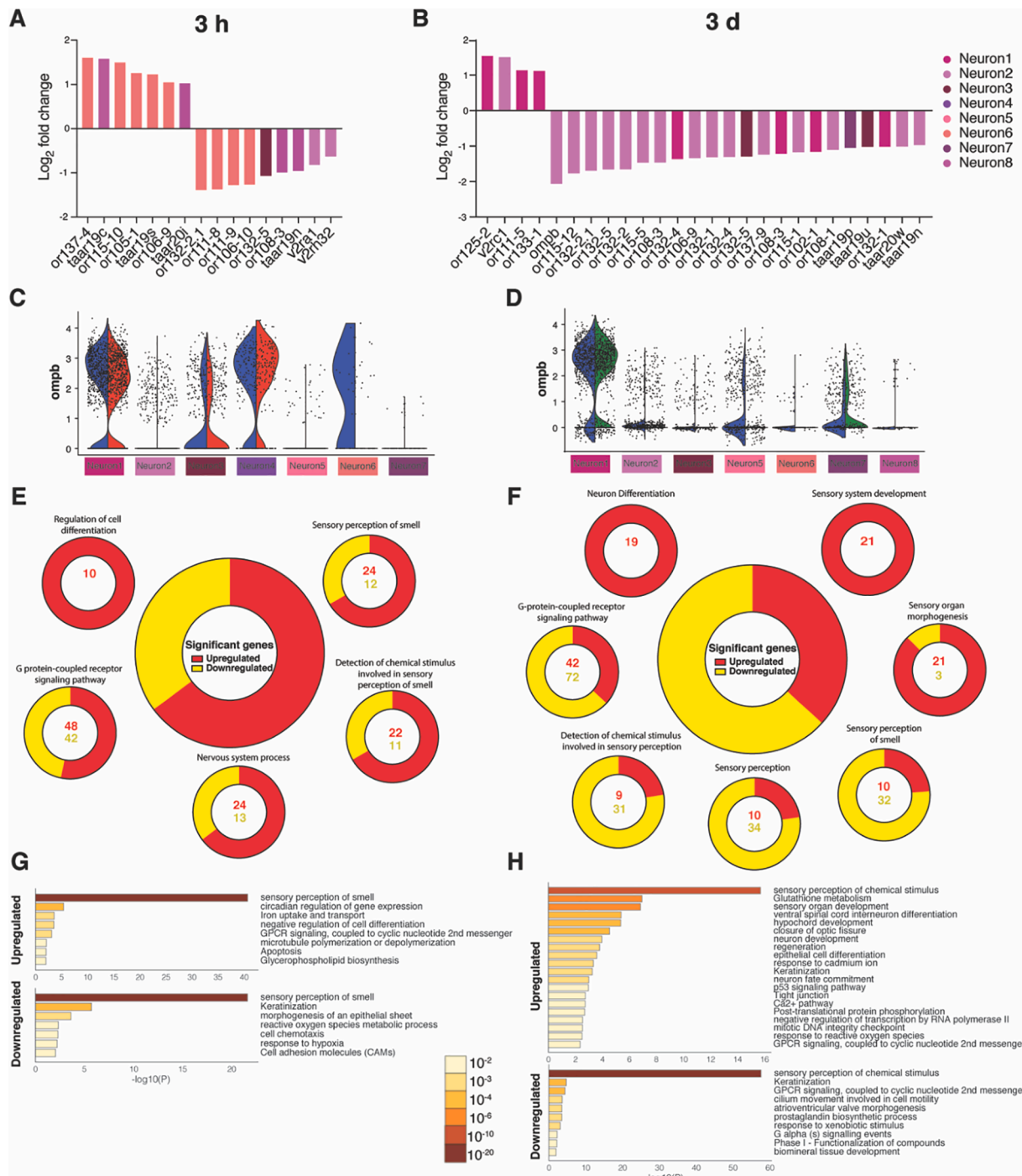

Fig. 5. Intranasal SARS-CoV-2 S RBD protein delivery causes widespread losses of olfactory receptor expression in adult zebrafish. (A-B) Bar plots showing fold-change in expression of olfactory receptor genes in the zebrafish OO 3 h and 3 d post intranasal SARS-CoV-2 S RBD protein compared to vehicle controls identified by scRNA-Seq. (C-D) Violin plots showing changes in significantly differentially expressed *ompb* expression, a marker of mature ciliated OSNs, in zebrafish OO cell suspensions, across all olfactory neuronal cell clusters in 3 h SARS-CoV-2 S RBD (orange) and 3 d SARS-CoV-2 S RBD (green) versus vehicle treated (blue). (E-F) Summary webs of gene ontology analyses performed in ShinyGO v0.61 from the scRNA-Seq data showing the number of significantly up and down regulated genes across olfactory neuronal clusters in zebrafish OO 3 h and 3 d post-intranasal SARS-CoV-2 S RBD protein versus vehicle treated controls. (G-H) Gene set enrichment analysis using Metascape of genes from all neuronal clusters that were either significantly up or down regulated in zebrafish OO 3 h and 3 d post-intranasal SARS-CoV-2 S RBD protein compared to vehicle treated controls (adjusted *P*-value < 0.05). Enriched terms are colored by *P*-value.

important cellular responses in neuronal and immune cell subsets of the zebrafish OO in response to SARS-CoV-2 S RBD.

Previous studies have blamed local inflammation of the olfactory mucosa as the main cause of anosmia in COVID-19 patients (Rodriguez et al., 2020; Torabi et al., 2020). We found transcriptional changes indicative of inflammation in the zebrafish OO treated with SARS-CoV-2 S RBD (Fig. 4E-F). By 3 h post I.N. delivery of recombinant SARS-CoV-2 S RBD, SCs and ECs showed significant increased expression of cytokine
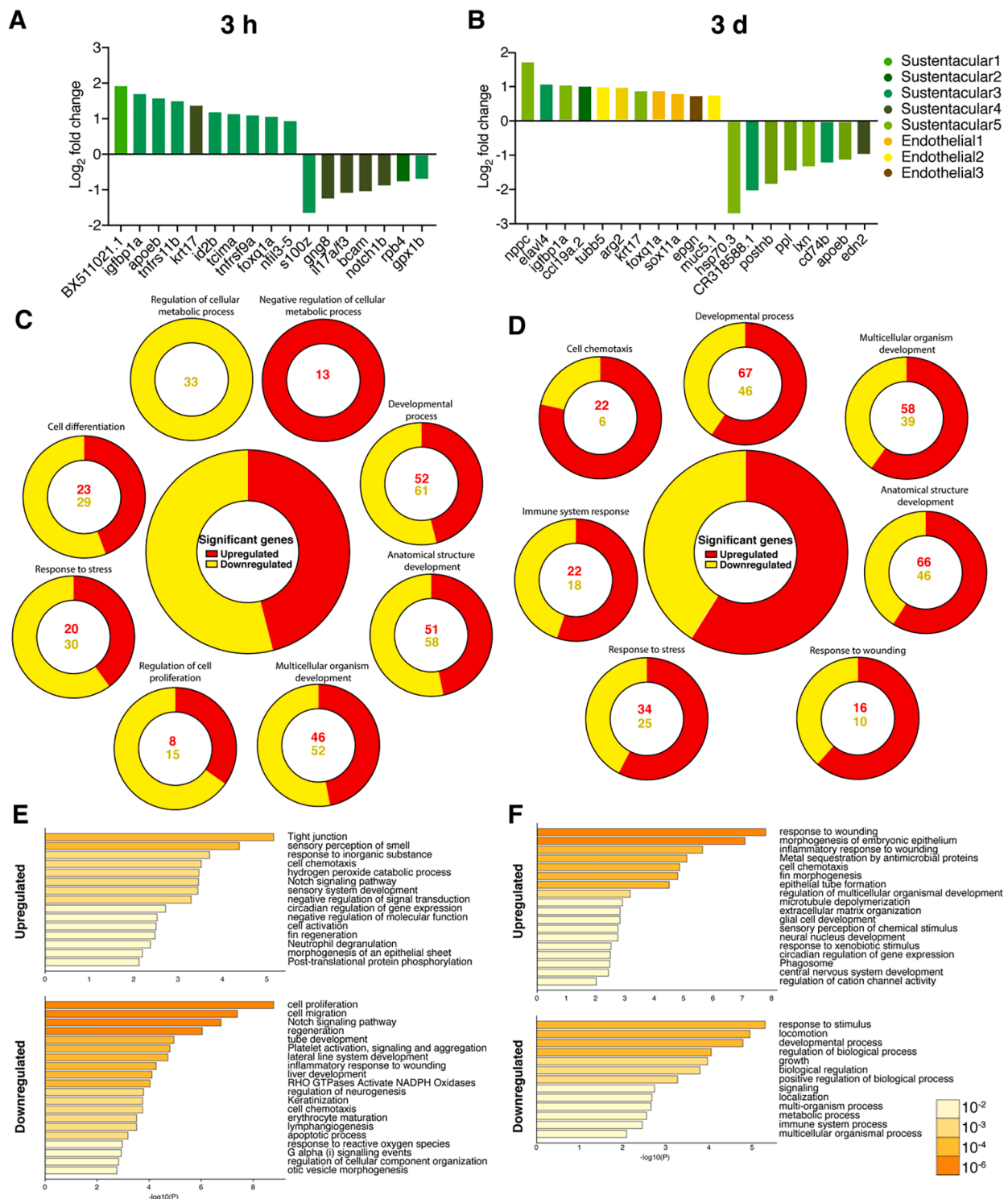

Fig. 6. Intranasal SARS-CoV-2 S RBD protein delivery causes transcriptional changes in zebrafish sustentacular and endothelial clusters. (A-B) Bar plots showing fold-change in expression of selected significantly differentially expressed genes in sustentacular and endothelial cell clusters in the zebrafish OO 3 h and 3 d post intranasal SARS-CoV-2 S RBD protein compared to vehicle controls identified by scRNA-Seq. (C-D) Summary webs of gene ontology analysis performed in Shiny-GO v0.61 from the scRNA-Seq data showing the number of genes significantly up and down regulated in sustentacular and endothelial cell clusters in the OO of zebrafish 3 h and 3 days post-intranasal SARS-CoV-2 S RBD protein compared to vehicle treated controls. (E-F) Gene set enrichment analysis using Metascape of genes from sustentacular and endothelial clusters that were either significantly up or down regulated in zebrafish OO 3 h and 3 d post-intranasal SARS-CoV-2 S RBD protein compared to vehicle treated controls (adjusted P-value < 0.05). Significantly enriched terms are colored by *P-value*.

genes (*il15, il4r,* and *ccl19b*) and prostaglandin I2 synthase (*ptgis*), while myeloid clusters upregulated expression of the interferon gene *irf1b* (Fig. 4E). Strikingly, NF-kB inhibitor alpha (*nfkbiaa*) was differentially expressed across almost all cell types including progenitor-like neuronal clusters at 3 h relative to vehicle control (Fig. 4E). By 3 d post-treatment, myeloid clusters expressed inflammatory markers (*il1b* and *tnfa*) and showed a significant differential upregulation of the chemokine receptor *cxcr4b* suggesting perhaps trafficking into the OO from other body sites (Fig. 4F). Because hemorrhages were observed in the OO at 3 h and 1 d by histology, we were not surprised to find significant differential expression of genes related to endothelial integrity including angiopoietin-like 4 (*angptl4*), angiomotin (*amotl2b*), and Wiskott-Aldrich syndrome protein (*wasb*) as well as other genes associated with vasoconstriction (*dusp5* and *vaspa*) at 3 h post I.N. delivery of SARS-CoV-2 S RBD (Fig. 4E) (Li et al., 2015; Wagener et al., 2016; Zheng et al., 2009). By 3 d after I.N. SARS-CoV-2 S RBD, endothelial clusters showed significantly increased expression of clotting factors (*f3b* and *f3a*) relative to vehicle treated control and continued upregulation of *angptl4* expression was detected in several EC and SC clusters (Fig. 4F). Thus, this data suggested that inflammatory responses and endothelial disruption are both hallmarks of SARS-CoV-2 S RBD induced damage in the olfactory epithelium.

Differential expression analysis revealed that while some changes in ORs expression occurred 3 h post-treatment in neuronal progenitor clusters, many ORs and TAARS genes were significantly differentially downregulated in mature neuronal clusters 1 and 2 compared to vehicle treated control (Fig. 5A-B). In accord, markers of mature ciliated and microvillus OSNs (*ompb* and *v2rh32,* respectively) were significantly downregulated at both 3 h and 3 d after I.N. SARS-CoV-2 S RBD delivery (Fig. 5A-D). We next used gene ontology (GO) analyses of significantly up or down regulated genes across neuronal clusters at 3 h or 3 d after treatment compared to vehicle treated controls (Fig. 5E-H) (Ge et al., 2020; Zhou et al., 2019). At 3 h after I.N. SARS-CoV-2 S RBD delivery, upregulated genes in the olfactory neuronal clusters were enriched in regulation of cell differentiation and sensory perception of smell (Fig. 5E). By 3 d, upregulated genes identified in olfactory neuronal clusters were enriched in processes such as neuron differentiation, sensory system development, and sensory organ morphogenesis. Interestingly, downregulated genes also belonged to sensory perception of smell, detection of chemical stimulus and GPCR signaling pathway (Fig. 5F). Functional enrichment analyses showed that the top non-redundant enriched clusters in both upregulated and downregulated genes in zebrafish OSNs 3 h post-treatment was sensory perception of smell (Fig. 5G). The same was true 3 d post-treatment although a more complex picture emerged, processes such as regeneration, neuron development, neuron fate commitment and the p53 signaling pathway also showed enrichment within the upregulated genes (Fig. 5H). Combined, these results suggest that presence of SARS-CoV-2 S RBD in the OO indirectly instigates harmful effects on OSNs within hours and activates numerous transcriptional pathways in neurons, sustentacular cells, endothelial cells and immune cells that are still noticeable at 3 d post-treatment. Further, these analyses indicate that neuronal regeneration and differentiation processes were occurring by 3 d likely as a way to assure tissue repair following olfactory damage.

3.7. Intranasal delivery of SARS-CoV-2 S RBD induces responses in sustentacular cells and endothelial cell clusters

Co-expression of *ace2* and *tmprss2* by olfactory SCs and basal cells in the human olfactory epithelium and subsequent onset of damage and inflammation of these cell subsets may explain olfactory loss in COVID-19 patients (Brann et al., 2020; Cooper et al., 2020; Muus et al., 2021; Sungnak et al., 2020). Additionally, *ace2* is expressed in ECs and these cells are infected by SARS-CoV-2 (Bryche et al., 2020). The single cell transcriptomic approach allowed us to dissect how each cell type in the zebrafish OO responds to SARS-CoV-2 S RBD and gain some mechanistic

insights into the cause of the olfactory dysfunction. Our results indicate unique responses by SC clusters and EC clusters to treatment (Figs. 4 and 6). At 3 h, we detected increased expression of *apoeb*, of transcription factors *foxq1a* and *id2b*, the transcriptional regulator *nfil3-5*, two tumor necrosis factor receptor superfamily members (*tnfrsf11b* and *tnfrsf9a*) as well as *tcima* (transcriptional and immune response regulator), whose mammalian ortholog *pcim* regulates immune responses as well as endothelial cell activation and expression of inflammatory genes (Fig. 6A) (Kim et al., 2009). Further, at 3 h we observed downregulation of the pro-inflammatory cytokine *il17af/3* as well as glutathione peroxidase *gpx1b,* the transcription factor *notch1b*, basal cell adhesion molecule *bcam*, guanine nucleotide-binding protein subunit gamma *gng8*, and the calcium binding *s100z* in SC and EC from SARS-CoV-2 S RBD treated OO relative to vehicle treated. At 3 d post-treatment, we observed significant increased expression of the gene that encodes brain natriuretic peptide (*nppc*), a vasodilating hormone, the pro-inflammatory chemokine *ccl19a.2,* the M2 macrophage marker *arg2,* the transcription factors *foxq1a* and *sox11a*, tubulin beta 5 *tubb5*, and the epithelial mitogen *epgn,* among others (Fig. 6B). Downregulated genes at 3 d post-treatment included *hsp70.3*, *apoeb*, the osteoblast specific factor b (*postb*), the desmosomal component periplakin (*ppl*), the vasoconstricting endothelin 2 (*edn2*), the heparin binding molecule latexin (*ltx*) involved in pain and inflammation, and *cd74b,* a part of the MHC-II complex (Fig. 6B). Combined, these data indicated immune regulatory responses in SC and EC clusters early after SARS-CoV-2 S RBD treatment, followed by transcriptional changes with potential vasoactive effects by day 3.

GO and enrichment set analyses indicated that SC and EC clusters initially undergo transcriptional changes enriched in metabolic responses, response to stress, and cell differentiation (Fig. 6C). Later on, at 3 d, SC and EC responses were enriched in genes involved not only in stress response but also in immune responses and responses to wounding (Fig. 6D). Similar results were identified using Metascape, which showed that the inflammatory response to wounding was moderately enriched in the downregulated genes at 3 h, whereas by day 3, response to wounding became the top enriched set among the upregulated genes (Fig. 6E-F).

4. Discussion

SARS-CoV-2 infection causes anosmia and ageusia (loss of taste) in 41–84% of patients (Dell'Era et al., 2020; Spinato et al., 2020; Parma et al., 2020; Sbrana et al., 2020). Several mechanisms for the impaired chemosensory perception in COVID-19 patients have been proposed based on the observation that, in humans, SCs and basal cells, but not OSNs, co-express *ace2* and *tmprss2* (Brann et al., 2020; Sungnak et al., 2020). Initial infection of SC but not OSNs appears to indirectly cause damage to OSNs, notably via lack of metabolic support or via inflammatory-derived damage (Brann et al., 2020; Khan et al., 2021a). Animal models of SARS-CoV-2 infection have provided insights into the mechanisms of olfactory loss driven by SARS-CoV-2, particularly the golden Syrian hamster (Bryche et al., 2020; Chan et al., 2020; Dias De Melo et al., 2021b). In the hamster model, I.N. SARS-CoV-2 infection results in drastic damage of the OE including ciliary loss and desquamation of cells into the nasal cavity (Zhang et al., 2020, Bryche et al., 2020). Behavioral assays also suggest functional loss of smell in the Syrian hamster SARS-CoV-2 infection model (Dias De Melo et al., 2021b; Zhang et al., 2020). Olfactory damage in this model appears to be transient since signs of recovery in the OE can be detected 7–14 d post-infection (Bryche et al, 2020) and full recovery has been proposed to occur 21 d post-infection (Urata et al., 2021). These results parallel smell recovery in most COVID-19 patients, which takes approximately 2 w (Gorzkowski et al., 2020; Mangia et al., 2021). Our results indicate that I.N. delivery of SARS-CoV-2 S RBD is sufficient to cause severe olfactory damage in adult zebrafish including loss of cilia, edema, hemorrhages and necrosis. SARS-CoV-2 S RBD clung to the apical regions of cells in

the non-sensory areas of the olfactory lamellae suggesting lack of direct interaction between SARS-CoV-2 S RBD and OSNs. In support, this exact same non-sensory area was apoptotic at 3 h and 3 d and proliferative by PCNA marker by 3 h and 3 d. Together, our data supports the idea that the interaction of SARS-CoV-2 S RBD with non-sensory regions of the zebrafish OO causes direct damage to this region, indirectly impacting OSN viability, OR expression, and OSN function resulting in severe olfactory dysfunction.

The findings of the current study are remarkably similar to those found in the golden Syrian hamster model during SARS-CoV-2 infection (Bryche et al., 2020). Complete loss of the neuroepithelium structure, exposing the lamina propria to the environment, occurred by 2 d post infection in the hamster model, while the SARS-CoV-2 S RBD was sufficient to cause the same damage by 3 h after administration in our study. Among the cellular changes recorded, staining with CTK8 revealed epithelial restructuring as early as 3 h post SARS-CoV-2 S RBD treatment. Similar losses in the olfactory mosaic pattern have been documented in the golden Syrian hamster model, where SCs are the cell type supporting infection (Bryche et al., 2020). Notably, CTK8 staining spread to the lamina propria compartment at 3 d post SARS-CoV-2 S RBD treatment, indicating a possible role for cytokeratin deposition in local olfactory tissue repair (Paladini et al., 1996; Usui et al., 2005). Of note, similar responses have been found in other zebrafish injury models (Calvo-Ochoa and Byrd-Jacobs, 2019; Martorana et al., 2001). Much of the damage in the lamina propria was vasculature hemorrhaging and widening particularly at 3 h, 1 d and 3 d after SARS-CoV-2 S RBD administration. This concurs with the presence of microthrombi in OE biopsies from COVID-19 patients (Kirschenbaum et al., 2020). scRNA-Seq revealed significantly differentially expressed genes associated with angiogenesis and clotting, which supported histological findings. Further, the lamina propria and raphe of the OO displayed eosinophilic swatches by 3 d and 5 d after SARS-CoV-2 S RBD treatment, that were likely keratin and not collagen based on Masson Trichome stains. The lamina propria contains axon bundles of OSNs projecting to the OB. Thus, damage of the connective tissue within which axons travel may well be a contributing cause of olfactory dysfunction in our model.

Our study indicates that olfactory histopathology in zebrafish treated with SARS-CoV-2 S RBD is coupled with aberrant olfactory function. We combined electrophysiology and behavior to capture the physiological responses to SARS-CoV-2 S RBD in adult zebrafish. Previous studies in K18-hACE2 mice show anosmia onset 2–3 d after SARS-CoV-2 infection (Zheng et al., 2020). In the golden Syrian hamster model, full regeneration at the histological level is completed 21 d post-infection and behavioral preference for food, lost early during infection, is recovered 14 d post-infection (Dias De Melo et al., 2021b). The present study determined that adult zebrafish recover olfactory function following SARS-CoV-2 S RBD I.N. treatment by 3 d, indicating that functional recovery occurs faster than in mammalian models. Interestingly, olfactory tissue damage was not fully repaired until 2 w post-treatment based on histopathology, an intriguing observation that deserves further investigation.

Our EOG data indicated global loss of olfaction in response to both food and bile odorants at 3 h and 1 d. Of the two predominant types of mature OSNs, ciliated OSNs respond to bile whereas microvillous OSNs respond to amino acids within food (Michel and Derbidge, 1997; Sato et al., 2005). Therefore, decreased electrical responses to both food and bile odorants suggests dysregulation of both types of neurons after SARS-CoV-2 S RBD administration and widespread OSN dysfunction concomitant with our scRNA-Seq results. Transcriptional profiles of OSNs revealed dramatic losses in OR expression as early as 3 h post-treatment; which correlated with functional loss of sense of smell by EOG. By 3 d post-treatment a global downregulation of ORs and VRs expression predicted defective sensory perception programs by gene ontology yet EOG results showed elevated rather than reduced responses to odorants. An EOG signal is a field response arising from the summation of local depolarizations and repolarizations of many OSNs and it

does not always correlate with histological observations as reported by others (Pozharskaya et al., 2013). Elevated EOG responses to odorants 3 d post-treatment indicate overcompensation of olfactory responses in our model. The vertebrate olfactory system displays remarkable compensatory plasticity (Waggener and Coppola, 2007). For instance, naris occlusion experiments in mice showed greater EOG amplitudes to odors in occluded compared to control olfactory epithelia (Waggener and Coppola, 2007). Additionally, SARS-CoV-2 S RBD treatment may impact metabolic signals which can result in altered EOG recordings including increased sensitivity to odorants (reviewed by Bryche et al., 2021). Finally, the global damage observed in the olfactory tissue at 3 d including changes in sustentacular cells and OSNs may alter transduction signaling in response to odorants, perhaps resulting in compensatory EOG responses.

Our model revealed dynamic cellular changes in the zebrafish OO following SARS-CoV-2 S RBD induced damage. Proliferation in the OO was observed with anti-PCNA stains at 3 h and 3 d after I.N. SARS-CoV-2 S RBD delivery. Activated caspase-3 staining revealed some degree of apoptosis in the OO of SARS-CoV-2 S RBD treated zebrafish, especially in the non-sensory regions where recombinant protein was mostly observed. However, since we did not co-stain with other cellular markers, we cannot determine at this time what cell types were undergoing apoptosis in this region. Activated caspase-3 reactivity was also sometimes located at the base of the neuroepithelium, suggesting perhaps apoptosis of progenitor cells such as horizontal or globose basal cells, a point that deserves careful future investigation. In studies of acute and chronic damage to the OE in mice, these basal cell types become immune effectors in addition to neural progenitors, and prolonged inflammation decreases regenerative abilities of the OO (Chen et al., 2019). In our acute model, scRNA-Seq revealed that intermediate neuronal precursor clusters rapidly expand after damage triggered by I. N. SAR-CoV-2 S RBD administration perhaps to replace lost mature OSNs. Future experiments will establish the dynamics of cell death in each olfactory cell subset during I.N. SARS-CoV-2 infection or SARS-CoV-2 S RBD delivery.

Inflammation in the OO may be sufficient to trigger anosmia as evidenced by recent work in mammalian models (Rodriguez et al., 2020). Our scRNA-Seq data also detected inflammatory gene signatures in SCs, ECs and myeloid cell subsets in animals treated with SARS-CoV-2 S RBD indicating that SARS-CoV-2 S RBD damage causes inflammation in a variety of cell types found in the olfactory epithelium. Thus, although direct interaction between SARS-CoV-2 S RBD was limited to non-sensory areas, the inflammatory milieu, therefore, may cause collateral damage on OSNs and result in aberrant olfactory function. Of interest, in the Syrian hamster model, an increase in Iba1$^+$ cells in the OO (Bryche et al., 2020) was observed. Similarly, we observed an increase in macrophages (myeloid3 subset) at 3 d. The spike protein has been shown to induce secretion of Il-1β and Il-6 in COVID-19 convalescent human macrophages and human epithelial cells, respectively (Patra et al., 2020; Theobald et al., 2021). Of note, we identified significant decreases in the proportions of T_{regs} in SARS-CoV-2 S RBD treated OO compared to controls at both time points examined. These results may suggest that inflammation could result from T_{reg} dysregulation, as in COVID-19 patients, who have decreased percentages of T_{regs} in circulation (Galván-Peña et al., 2020; Rahimzadeh and Naderi, 2021).

Further studies are warranted to understand how olfactory function is altered by SARS-CoV-2 S RBD. We detected *ace2* expression in the OO and, to a lesser degree the OB, of adult zebrafish. Further, we detected the SARS-CoV-2 S RBD protein associated with the non-sensory epithelium of the OO but not regions where OSNs are present. Thus, at this point, we cannot conclude whether Ace2 mediates the damage caused by SARS-CoV-2 S RBD since we did not test internalization of zebrafish ACE2 following SARS-CoV-2 S RBD treatment. The SARS-CoV-2 S RBD alone has been shown to internalize, co-localized to ACE2, in cell culture studies and it caused increased permeability of brain microvascular endothelial cells offering multiple potential avenues for entry into the

OO (Gorshkov et al., 2020; Raghavan et al., 2021; Wang et al., 2008; Zheng et al., 2021). Addition of the SARS-CoV-2 RBD protein has been shown to increase TNF-α production in endothelial cells and activate NF-κB directed inflammation, while viral infection has been credited with causing cytokine chaos in COVID-19 patients (Cao et al., 2021; Haga et al., 2008; Khan et al., 2021b; Lucas et al., 2020). Our scRNA-Seq study did show differential upregulation of inflammatory cytokines across immune and epithelial cell types (Fig. 4E-F). Of note, human COVID-19 patients present viral infected olfactory epithelial cells with high expression of neuropilin-1, a receptor that facilitates SARS-CoV-2 entry to the OSNs (Cantuti-Castelvetri et al., 2020). Additionally, the olfactory tissue by nature is capable of interacting with a plethora of molecular patterns as odorants (Friedrich, 2006). Thus, we cannot rule out that mechanisms independent of ACE2 may be playing a role in our model. Zebrafish ACE2 antibody blocking experiments and/or use of zebrafish ACE2 mutant lines may shed light the direct mechanism by which SARS-CoV-2 S RBD is connected to inflammation, olfactory dysfunction and tissue damage in the OO.

A recent report in zebrafish adults indicated that injection of recombinant SARS-CoV-2 S N terminal protein caused histopathology of several tissues including the liver, kidney, brain and ovary (Ventura-Fernandes et al., 2020). Additionally, some animals succumbed to injection with the recombinant protein. In adults, we did not detect mortalities in any of our experiments, perhaps suggesting that mortalities were due to the injection procedure rather than the protein treatment. Of note, the dose used in the present study was considerably lower than the dose delivered in the Ventura-Fernandez study, perhaps explaining the differences in toxicity between both studies. Thus, toxicity of SARS-CoV-2 S protein in adult zebrafish may be less severe when delivered I.N. than by injection, and future studies should evaluate whether current vaccine candidates also exert similar effects and whether different administration routes cause the same side-effects or not. This is particularly important as the I.N. route appears promising for some vaccine candidates (Alu et al., 2022; Ku et al., 2020). A recent preclinical study shows that an I.N. adenovirus vectored SARS-CoV-2 vaccine reduces the amount of viable virions shed by both Syrian golden hamsters and macaques after challenge with SARS-CoV-2 D614G, but the effects of I.N vaccination on olfactory function were not evaluated (Van Doremalen et al., 2021). Further, an I.N. vaccine consisting of chitosan nanoparticles to deliver synthetic peptide epitopes for SARS-CoV-2 RBD has thus far found no signs of olfactory impairment in humans (RaDVaC, 2021). More work is warranted to understand whether SARS-CoV-2 RBD is sufficient to cause anosmia or not in humans. The construction of a humanized ACE2 zebrafish model will allow further mechanistic studies.

In conclusion, our work demonstrates that a fragment of SARS-CoV-2 S1 protein, the RBD, can cause olfactory pathology and loss of smell in adult zebrafish. Our results support the notion that viral-derived proteins such as SARS-CoV-2 S RBD can have neurotoxic effects. The present study raises important questions pertaining to biochemical interactions of S1 and S1-derived protein fragments once a host is infected with SARS-CoV-2. If release of RBD or other S1 fragments occurs *in vivo*, the presence of free viral proteins may contribute or exacerbate viral pathophysiological damage. Further studies are warranted to provide experimental support for this hypothesis.

CRediT authorship contribution statement

Aurora Kraus: Conceptualization, Methodology, Investigation, Writing – original draft, Writing – review & editing. **Mar Huertas:** Conceptualization, Methodology, Investigation, Funding acquisition, Resources, Writing – review & editing. **Laura Ellis:** Investigation, Writing – review & editing. **Pierre Boudinot:** Conceptualization, Writing – review & editing. **Jean-Pierre Levraud:** Conceptualization, Methodology, Investigation, Resources, Writing – review & editing. **Irene Salinas:** Conceptualization, Methodology, Investigation, Writing

– original draft, Funding acquisition, Resources, Supervision, Writing – review & editing.

Appendix A. Supplementary data

Supplementary data to this article can be found online at https://doi.org/10.1016/j.bbi.2022.03.006.

References

Alu, A., Chen, L., Lei, H., Wei, Y., Tian, X., Wei, X., 2022. Intranasal COVID-19 vaccines: From bench to bed. Lancet 76. https://doi.org/10.1016/j.ebiom.2022.103841.
Amanat, F., Stadlbauer, D., Strohmeier, S., Nguyen, T.H.O., Chromikova, V., McMahon, M., Jiang, K., Arunkumar, G.A., Jurczyszak, D., Polanco, J., Bermudez-Gonzalez, M., Kleiner, G., Aydillo, T., Miorin, L., Fierer, D.S., Lugo, L.A., Kojic, E.M., Stoever, J., Liu, S.T.H., Cunningham-Rundles, C., Felgner, P.L., Moran, T., García-Sastre, A., Caplivski, D., Cheng, A.C., Kedzierska, K., Vapalahti, O., Hepojoki, J.M., Simon, V., Krammer, F., 2020. A serological assay to detect SARS-CoV-2 seroconversion in humans. Nat. Med. 26 (7), 1033–1036. https://doi.org/10.1038/s41591-020-0913-5.
Ankel, H., Capobianchi, M.R., Castilletti, C., Dianzani, F., 1994. Interferon induction by HIV glycoprotein 120: role of the V3 loop. Virology 205, 34–43. https://doi.org/10.1006/viro.1994.1617.
Bansal, A.K., Mactutus, C.F., Nath, A., Maragos, W., Hauser, K.F., Booze, R.M., 2000. Neurotoxicity of HIV-1 proteins gp120 and Tat in the rat striatum. Brain Res. 879 (1-2), 42–49. https://doi.org/10.1016/S0006-8993(00)02725-6.
Beigmohammadi, M.T., Jahanbin, B., Safaei, M., Amoozadeh, L., Khoshavi, M., Mehrtash, V., Jafarzadeh, B., Abdollahi, A., 2020. Pathological Findings of Postmortem Biopsies From Lung, Heart, and Liver of 7 Deceased COVID-19 Patients. Int. J. Surg. Pathol. 29 (2), 135–145. https://doi.org/10.1177/1066896920935195.
Bergsland, M., Werme, M., Malewicz, M., Perlmann, T., Muhr, J., 2006. The establishment of neuronal properties is controlled by Sox4 and Sox11. Genes Dev. 20 (24), 3475–3486. https://doi.org/10.1101/gad.403406.
Bermingham-McDonogh, O., Reh, T.A., 2011. Regulated reprogramming in the regeneration of sensory receptor cells. Neuron 71 (3), 389–405. https://doi.org/10.1016/j.neuron.2011.07.015.
Bettini, S., Lazzari, M., Ferrando, S., Gallus, L., Franceschini, V., 2016. Histopathological analysis of the olfactory epithelium of zebrafish (Danio rerio) exposed to sublethal doses of urea. J. Anat. 228 (1), 59–69. https://doi.org/10.1111/joa.12397.
Borders, A.S., Hersh, M.A., Getchell, M.L., van Rooijen, N., Cohen, D.A., Stromberg, A.J., Getchell, T.V., 2007. Macrophage-mediated neuroprotection and neurogenesis in the olfactory epithelium. Physiol. Genomics 31 (3), 531–543. https://doi.org/10.1152/physiolgenomics.00008.2007.
Brann, D.H., Tsukahara, T., Weinreb, C., Lipovsek, M., Van Den Berge, K., Gong, B., Chance, R., Macaulay, I.C., Chou, H.J., Fletcher, R.B., Das, D., Street, K., De Bezieux, H.R., Choi, Y.G., Risso, D., Dudoit, S., Purdom, E., Mill, J., Hachem, R.A., Matsunami, H., Logan, D.W., Goldstein, B.J., Grubb, M.S., Ngai, J., Datta, S.R., 2020. Non-neuronal expression of SARS-CoV-2 entry genes in the olfactory system suggests mechanisms underlying COVID-19-associated anosmia. Sci. Adv. 6, eabc5801. https://doi.org/10.1126/sciadv.abc5801.
Bryche, B., St Albin, A., Murri, S., Lacôte, S., Pulido, C., Ar Gouilh, M., Lesellier, S., Servat, A., Wasniewski, M., Picard-Meyer, E., Monchatre-Leroy, E., Volmer, R.,

Rampin, O., Le Goffic, R., Marianneau, P., Meunier, N., 2020. Massive transient damage of the olfactory epithelium associated with infection of sustentacular cells by SARS-CoV-2 in golden Syrian hamsters. Brain. Behav. Immun. 89, 579–586. https://doi.org/10.1016/j.bbi.2020.06.032.

Bryche, B., Baly, C., Meunier, N., 2021. Modulation of olfactory signal detection in the olfactory epithelium: focus on the internal and external environment, and the emerging role of the immune system. Cell Tissue Res. 384 (3), 589–605. https://doi.org/10.1007/s00441-021-03467-y.

Buchinger, T.J., Li, K., Huertas, M., Baker, C.F., Jia, L., Hayes, M.C., Li, W., Johnson, N. S., 2017. Evidence for partial overlap of male olfactory cues in lampreys. J. Exp. Biol. 220, 497–506. https://doi.org/10.1242/jeb.149807.

Buiakova, O.I., Baker, H., Scott, J.W., Farbman, A., Kream, R., Grillo, M., Franzen, L., Richman, M., Davis, L.M., Abbondanzo, S., Stewart, C.L., Margolis, F.L., 1996. Olfactory marker protein (OMP) gene deletion causes altered physiological activity of olfactory sensory neurons. Proc. Natl. Acad. Sci. U. S. A. 93 (18), 9858–9863. https://doi.org/10.1073/pnas.93.18.9858.

Burgos, J.S., Ripoll-Gomez, J., Alfaro, J.M., Sastre, I., Valdivieso, F., 2008. Zebrafish as a New Model for Herpes Simplex Virus Type 1 Infection. Zebrafish 5, 323–333. https://doi.org/10.1089/zeb.2008.0552.

Butler, A., Hoffman, P., Smibert, P., Papalexi, E., Satija, R., 2018. Integrating single-cell transcriptomic data across different conditions, technologies, and species. Nat. Biotechnol. 36 (5), 411–420. https://doi.org/10.1038/nbt.4096.

Byrd, C.A., Brunjes, P.C., 1995. Organization of the olfactory system in the adult zebrafish: Histological, immunohistochemical, and quantitative analysis. J. Comp. Neurol. 358, 247–259. https://doi.org/10.1002/cne.903580207.

Calvo-Ochoa, E., Byrd-Jacobs, C.A., 2019. The olfactory system of zebrafish as a model for the study of neurotoxicity and injury: Implications for neuroplasticity and disease. Int. J. Mol. Sci. 20, 1639. https://doi.org/10.3390/ijms20071639.

Campanella, J.J., Bitincka, L., Smalley, J., 2003. MatGAT: An application that generates similarity/identity matrices using protein or DNA sequences. BMC Bioinformatics 4. https://doi.org/10.1186/1471-2105-4-29.

Cantuti-Castelvetri, L., Ojha, R., Pedro, L.D., Djannatian, M., Franz, J., Kuivanen, S., van der Meer, F., Kallio, K., Kaya, T., Anastasina, M., Smura, T., Levanov, L., Szirovicza, L., Tobi, A., Kallio-Kokko, H., Österlund, P., Joensuu, M., Meunier, Frédéric.A., Butcher, S.J., Winkler, M.S., Mollenhauer, B., Helenius, A., Gokce, O., Teesalu, T., Hepojoki, J., Vapalahti, O., Stadelmann, C., Balistreri, G., Simons, M., 2020. Neuropilin-1 facilitates SARS-CoV-2 cell entry and infectivity. Science (80-. 370 (6518), 856–860. https://doi.org/10.1126/science:abd2985.

Cao, X., Tian, Y., Nguyen, V., Zhang, Y., Gao, C., Yin, R., Carver, W., Fan, D., Albrecht, H., Cui, T., Tan, W., 2021. Spike protein of SARS-CoV-2 activates macrophages and contributes to induction of acute lung inflammation in male mice. FASEB 35 (9). https://doi.org/10.1096/fsb2.v35.910.1096/fj.202002742RR.

Carignan, A., Valiquette, L., Grenier, C., Musonera, J.B., Nkengurutse, D., Marcil-Héguy, A., Vettese, K., Marcoux, D., Valiquette, C., Xiong, W.T., Fortier, P.-H., Généreux, Mélissa, Pépin, J., 2020. Anosmia and dysgeusia associated with SARS-CoV-2 infection: an age-matched case−control study. Cmaj 192 (26), E702–E707. https://doi.org/10.1503/cmaj.200869.

Casadei, E., Tacchi, L., Lickwar, C.R., Espenschied, S.T., Davison, J.M., Muñoz, P., Rawls, J.F., Salinas, I., 2019. Commensal Bacteria Regulate Gene Expression and Differentiation in Vertebrate Olfactory Systems Through Transcription Factor REST. Chem. Senses 44, 615–629. https://doi.org/10.1093/chemse/bjz050.

Chan, J.F.W., Zhang, A.J., Yuan, S., Poon, V.K.M., Chan, C.C.S., Lee, A.C.Y., Chan, W.M., Fan, Z., Tsoi, H.W., Wen, L., Liang, R., Cao, J., Chen, Y., Tang, K., Luo, C., Cai, J.P., Kok, K.H., Chu, H., Chan, K.H., Sridhar, S., Chen, Z., Chen, H., To, K.K.W., Yuen, K. Y., 2020. Simulation of the clinical and pathological manifestations of Coronavirus Disease 2019 (COVID-19) in golden Syrian hamster model: implications for disease pathogenesis and transmissibility. Clin. Infect. Dis. 2019 https://doi.org/10.1093/cid/ciaa325.

Chen, M., Reed, R.R., Lane, A.P., 2019. Chronic Inflammation Directs an Olfactory Stem Cell Functional Switch from Neuroregeneration to Immune Defense. Cell Stem Cell 25 (4), 501–513.e5. https://doi.org/10.1016/j.stem.2019.08.011.

Chen, M., Reed, R.R., Lane, A.P., 2017. Acute inflammation regulates neuroregeneration through the NF-κB pathway in olfactory epithelium. Proc. Natl. Acad. Sci. 114 (30), 8089–8094. https://doi.org/10.1073/pnas.1620664114.

Chen, R., Wang, K., Yu, J., Howard, D., French, L., Chen, Z., Wen, C., Xu, Z., 2021. The Spatial and Cell-Type Distribution of SARS-CoV-2 Receptor ACE2 in the Human and Mouse Brains. Front. Neurol. 11, 573095 https://doi.org/10.3389/fneur.2020.573095.

Chenna, R., Sugawara, H., Koike, T., Lopez, R., Gibson, T.J., Higgins, D.G., Thompson, J. D., 2003. Multiple sequence alignment with the Clustal series of programs. Nucleic Acids Res. 31, 3497–3500. https://doi.org/10.1093/nar/gkg500.

Chung, T.W.H., Sridhar, S., Zhang, A.J., Chan, K.H., Li, H.L., Wong, F.K.C., Ng, M.Y., Tsang, R.K.Y., Lee, A.C.Y., Fan, Z., Ho, R.S.L., Luk, S.Y., Kan, W.K., Lam, S.H.Y., Wu, A.K.L., Leung, S.M., Chan, W.M., Ng, P.Y., To, K.K.W., Cheng, V.C.C., Lung, K.C., Hung, I.F.N., Yuen, K.Y., 2020. Olfactory Dysfunction in Coronavirus Disease 2019 Patients: Observational Cohort Study and Systematic Review. Open Forum. Infect. Dis. 7, ofaa199. https://doi.org/10.1093/ofid/ofaa199.

Cooper, K.W., Brann, D.H., Farruggia, M.C., Bhutani, S., Pellegrino, R., Tsukahara, T., Weinreb, C., Joseph, P.V., Larson, E.D., Parma, V., Albers, M.W., Barlow, L.A., Datta, S.R., Di Pizio, A., 2020. COVID-19 and the Chemical Senses: Supporting Players Take Center Stage. Neuron 107, 219–233. https://doi.org/10.1016/j.neuron.2020.06.032.

Costa, K.C.M., Brigante, T.A.V., Fernandes, G.G., Scomparin, D.S., Scarante, F.F., de Oliveira, D.P., Campos, A.C., 2021. Zebrafish as a translational model: An experimental alternative to study the mechanisms involved in anosmia and possible

neurodegenerative aspects of covid-19? eNeuro 8, 1–17. https://doi.org/10.1523/ENEURO.0027-21.2021.

Damas, J., Hughes, G.M., Keough, K.C., Painter, C.A., Persky, N.S., Corbo, M., Hiller, M., Koepfli, K.P., Pfenning, A.R., Zhao, H., Genereux, D.P., Swofford, R., Pollard, K.S., Ryder, O.A., Nweeia, M.T., Lindblad-Toh, K., Teeling, E.C., Karlsson, E.K., Lewin, H. A., 2020. Broad host range of SARS-CoV-2 predicted by comparative and structural analysis of ACE2 in vertebrates. Proc. Natl. Acad. Sci. U.S.A. 117, 22311–22322. https://doi.org/10.1073/pnas.2010146117.

de Melo, G.D., Lazarini, F., Levallois, S., Hautefort, C., Michel, V., Larrous, F., Verillaud, B., Aparicio, C., Wagner, S., Gheusi, G., Kergoat, L., Kornobis, E., Donati, F., Cokelaer, T., Hervochon, R., Madec, Y., Roze, E., Salmon, D., Bourhy, H., Lecuit, M., Lledo, P.-M., 2021a. COVID-19-related anosmia is associated with viral persistence and inflammation in human olfactory epithelium and brain infection in hamsters. Sci. Transl. Med. 10, 1126. https://doi.org/10.1126/scitranslmed.abf8396.

Dell'Era, V., Farri, F., Garzaro, G., Gatto, M., Aluffi Valletti, P., M., Garzaro, 2020. Smell and taste disorders during COVID-19 outbreak: Cross-sectional study on 355 patients. Head Neck 42, 1591–1596. https://doi.org/10.1002/hed.26288.

de Melo, G.D., Lazarini, F., Levallois, S., Hautefort, C., Michel, V., Larrous, F., Verillaud, B., Aparicio, C., Wagner, S., Gheusi, G., Kergoat, L., Kornobis, E., Donati, F., Cokelaer, T., Hervochon, Rémi, Madec, Y., Roze, E., Salmon, D., Bourhy, H., Lecuit, M., Lledo, P.-M., 2021b. COVID-19-related anosmia is associated with viral persistence and inflammation in human olfactory epithelium and brain infection in hamsters. Science (80-. 13 (596) https://doi.org/10.1126/scitranslmed.abf8396.

Eliezer, M., Hautefort, C., Hamel, A.-L., Verillaud, B., Herman, P., Houdart, E., Eloit, C., 2020. Sudden and Complete Olfactory Loss of Function as a Possible Symptom of COVID-19. JAMA Otolaryngol Head Neck Surg 146, 674–675. https://doi.org/10.1001/jamaoto.2020.0832.

Ellett, F., Pase, L., Hayman, J.W., Andrianopoulos, A., Lieschke, G.J., 2011. Mpeg1 Promoter Transgenes Direct Macrophage-Lineage Expression in Zebrafish. Blood 117, 49–56. https://doi.org/10.1182/blood-2010-10-314120.

François, A., Grebert, D., Rhimi, M., Mariadassou, M., Naudon, L., Rabot, S., Meunier, N., 2016. Olfactory epithelium changes in germfree mice. Sci. Rep. 6, 24687. https://doi.org/10.1038/srep24687.

Friedrich, R.W., 2006. Mechanisms of odor discrimination: neurophysiological and behavioral approaches. Trends Neurosci. 29 (1), 40–47. https://doi.org/10.1016/j.tins.2005.10.004.

Gabor, K.A., Goody, M.F., Witten, P.E., Mowel, W.K., Breitbach, M.E., Kim, C.H., Gratacap, R.L., 2014. Influenza A virus infection in zebrafish recapitulates mammalian infection and sensitivity to anti-influenza drug treatment. Dis. Model. Mech. 7, 1227–1237. https://doi.org/10.1242/dmm.014746.

Galindo-Villegas, J., 2020. COVID-19: Real-time dissemination of scientific information to fight a public health emergency of international concern. Front. Pharmacol. 14 (1), 1–2. https://doi.org/10.5582/bst.2020.01056.

Galván-Peña, S., Leon, J., Chowdhary, K., Michelson, D.A., Vijaykumar, B., Yang, L., Magnuson, A., Manickas-Hill, Z., Piechocka-Trocha, A., Worrall, D.P., Hall, K.E., Ghebremichael, M., Walker, B.D., Li, J.Z., Yu, X.G., 2020. Profound Treg perturbations correlate with COVID-19 severity. BioRxiv. https://doi.org/10.1101/2020.12.11.416180.

Ge, S.X., Jung, D., Yao, R., 2020. ShinyGO: a graphical gene-set enrichment tool for animals and plants. Bioinformatics 36, 2628–2629. https://doi.org/10.1093/bioinformatics/btz931.

Giancotti, V., Bergamin, N., Cataldi, P., Rizzi, C., 2018. Epigenetic Contribution of High-Mobility Group A Proteins to Stem Cell Properties. Int. J. Cell Biol. 2018, 1–20. https://doi.org/10.1155/2018/3698078.

Gomes, M.C., Mostowy, S., 2020. The Case for Modeling Human Infection in Zebrafish. Trends Microbiol. 28 (1), 10–18. https://doi.org/10.1016/j.tim.2019.08.005.

Gorshkov, K., Susumu, K., Chen, J., Xu, M., Pradhan, M., Zhu, W., Hu, X., Breger, J.C., Wolak, M., Oh, E., 2020. Quantum Dot-Conjugated SARS-CoV - 2 Spike Pseudo-Virions Enable Tracking of Angiotensin Converting Enzyme 2 Binding and Endocytosis. ACS Nano 14 (9), 12234–12247. https://doi.org/10.1021/acsnano.0c05975.

Gorzkowski, V., Bevilacqua, S., Charmillon, A., Jankowski, R., Gallet, P., Rumeau, C., Nguyen, D.T., 2020. Evolution of Olfactory Disorders in COVID-19 Patients. Laryngoscope 130, 2667–2673. https://doi.org/10.1002/lary.28957.

Haga, S., Yamamoto, N., Nakai-murakami, C., Osawa, Y., Tokunaga, K., Sata, T., 2008. Modulation of TNF-a-converting enzyme by the spike protein of SARS-CoV and ACE2 induces TNF-a production adn facilitates viral entry. PNAS 105, 7809–7814.

Hansen, A., Rolen, S.H., Anderson, K., Morita, Y., Caprio, J., Finger, T.E., 2003. Correlation between Olfactory Receptor Cell Type and Function in the Channel Catfish. J. Neurosci. 23 (28), 9328–9339. https://doi.org/10.1523/JNEUROSCI.23-28-09328.2003.

Hansen, A., Zeiske, E., 1998. The peripheral olfactory organ of the zebrafish, Danio rerio: An ultrastructural study. Chem. Senses 23 (1), 39–48. https://doi.org/10.1093/chemse/23.1.39.

Haugarvoll, E., Bjerkås, I., Nowak, B.F., Hordvik, I., Koppang, E.O., 2008. Identification and characterization of a novel intraepithelial lymphoid tissue in the gills of Atlantic salmon. J. Anat. 213, 202–209. https://doi.org/10.1111/j.1469-7580.2008.00943.x.

Hoffmann, M., Kleine-Weber, H., Pöhlmann, S., 2020a. A Multibasic Cleavage Site in the Spike Protein of SARS-CoV-2 Is Essential for Infection of Human Lung Cells. Mol. Cell 78 (4), 779–784.e5. https://doi.org/10.1016/j.molcel.2020.04.022.

Hoffmann, M., Kleine-Weber, H., Schroeder, S., Krüger, N., Herrler, T., Erichsen, S., Schiergens, T.S., Herrler, G., Wu, N.-H., Nitsche, A., Müller, M.A., Drosten, C., Pöhlmann, S., 2020b. SARS-CoV-2 Cell Entry Depends on ACE2 and TMPRSS2 and Is

Blocked by a Clinically Proven Protease Inhibitor. Cell 181 (2), 271–280.e8. https://doi.org/10.1016/j.cell.2020.02.052.

Holz, C.L., Nelli, R.K., Eilidh Wilson, M., Zarski, L.M., Azab, W., Baumgardner, R., Osterrieder, N., Pease, A., Zhang, L., Hession, S., Goehring, L.S., Hussey, S.B., Hussey, G.S., 2017. Viral genes and cellular markers associated with neurological complications during herpesvirus infections. J. Gen. Virol. 98, 1439–1454. https://doi.org/10.1099/jgv.0.000773.

Howe, K., Clark, M.D., Torroja, C.F., Torrance, J., Berthelot, C., Muffato, M., Collins, J.E., Humphray, S., McLaren, K., Matthews, L., McLaren, S., Sealy, I., Caccamo, M., Churcher, C., Scott, C., Barrett, J.C., Koch, R., Rauch, G.-Jörg., White, N., Chow, W., Kilian, B., Quintais, L.T., Guerra-Assunção, José.A., Zhou, Y., Gu, Y., Yen, J., Vogel, J.-H., Eyre, T., Redmond, S., Banerjee, R., Chi, J., Fu, B., Langley, E., Maguire, S.F., Laird, G.K., Lloyd, D., Kenyon, E., Donaldson, S., Sehra, H., Almeida-King, J., Loveland, J., Trevanion, S., Jones, M., Quail, M., Willey, D., Hunt, A., Burton, J., Sims, S., McLay, K., Plumb, B., Davis, J., Clee, C., Oliver, K., Clark, R., Riddle, C., Elliott, D., Threadgold, G., Harden, G., Ware, D., Begum, S., Mortimore, B., Kerry, G., Heath, P., Phillimore, B., Tracey, A., Corby, N., Dunn, M., Johnson, C., Wood, J., Clark, S., Pelan, S., Griffiths, G., Smith, M., Glithero, R., Howden, P., Barker, N., Lloyd, C., Stevens, C., Harley, J., Holt, K., Panagiotidis, G., Lovell, J., Beasley, H., Henderson, C., Gordon, D., Auger, K., Wright, D., Collins, J., Raisen, C., Dyer, L., Leung, K., Robertson, L., Ambridge, K., Leongamornlert, D., McGuire, S., Gilderthorp, R., Griffiths, C., Manthravadi, D., Nichol, S., Barker, G., Whitehead, S., Kay, M., Brown, J., Murnane, C., Gray, E., Humphries, M., Sycamore, N., Barker, D., Saunders, D., Wallis, J., Babbage, A., Hammond, S., Mashreghi-Mohammadi, M., Barr, L., Martin, S., Wray, P., Ellington, A., Matthews, N., Ellwood, M., Woodmansey, R., Clark, G., Cooper, J.D., Tromans, A., Grafham, D., Skuce, C., Pandian, R., Andrews, R., Harrison, E., Kimberley, A., Garnett, J., Fosker, N., Hall, R., Garner, P., Kelly, D., Bird, C., Palmer, S., Gehring, I., Berger, A., Dooley, C.M., Ersan-Ürün, Zübeyde, Eser, C., Geiger, H., Geisler, M., Karotki, L., Kirn, A., Konantz, J., Konantz, M., Oberländer, M., Rudolph-Geiger, S., Teucke, M., Lanz, C., Raddatz, Günter, Osoegawa, K., Zhu, B., Rapp, A., Widaa, S., Langford, C., Yang, F., Schuster, S.C., Carter, N.P., Harrow, J., Ning, Z., Herrero, J., Searle, S.M.J., Enright, A., Geisler, R., Plasterk, R.H.A., Lee, C., Westerfield, M., de Jong, P.J., Zon, L.I., Postlethwait, J.H., Nüsslein-Volhard, C., Hubbard, T.J.P., Crollius, H.R., Rogers, J., Stemple, D.L., 2013. The zebrafish reference genome sequence and its relationship to the human genome. Nature 496 (7446), 498–503. https://doi.org/10.1038/nature12111.

Imam, S.A., Lao, W.P., Reddy, P., Nguyen, S.A., Schlosser, R.J., 2020. Is SARS-CoV-2 (COVID-19) postviral olfactory dysfunction (PVOD) different from other PVOD? World. J. Otorhinolaryngol. - Head Neck Surg. 6, S26–S32. https://doi.org/10.1016/j.wjorl.2020.05.004.

Jia, K., Cheng, B., Huang, L., Xiao, J., Bai, Z., Liao, X., Cao, Z., Shen, T., Zhang, C., Hu, C., Lu, H., 2020. Thiophanate-methyl induces severe hepatotoxicity in zebrafish. Chemosphere 248, 125941. https://doi.org/10.1016/j.chemosphere.2020.125941.

Jutfelt, F., Sundin, J., Raby, G.D., Krång, A., Clark, T.D., Reynolds, J., 2017. Two-current choice flumes for testing avoidance and preference in aquatic animals. Methods Ecol. Evol. 8 (3), 379–390. https://doi.org/10.1111/mee3.2017.8.issue-310.1111/2041-210X.12668.

Kanaya, K., Kondo, K., Suzukawa, K., Sakamoto, T., Kikuta, S., Okada, K., Yamasoba, T., 2014. Innate immune responses and neuroepithelial degeneration and regeneration in the mouse olfactory mucosa induced by intranasal administration of Poly(I:C). Cell Tissue Res. 357, 279–299. https://doi.org/10.1007/s00441-014-1848-2.

Kermen, F., Franco, L.M., Wyatt, C., Yaksi, E., Brunjes, P., 2013. Neural circuits mediating olfactory-driven behavior in fish. Front. Neural Circuits 7, 55–61. https://doi.org/10.3389/fncir.2013.00062.

Khan, S., Shafiei, M.S., Longoria, C., Schoggins, J., Savani, R.C., Zaki, H., 2021a. SARS-CoV-2 spike protein induces inflammation via TLR2-dependent activation of the NF-kB pathway. bioRxiv. https://doi.org/10.1101/2021.03.16.435700.

Khan, M., Yoo, S.J., Clijsters, M., Backaert, W., Vanstapel, A., Speleman, K., Lietaer, C., Choi, S., Hether, T.D., Marcelis, L., Nam, A., Pan, L., Reeves, J.W., Van Bulck, P., Zhou, H., Bourgeois, M., Debaveye, Y., De Munter, P., Gunst, J., Jorissen, M., Lagrou, K., Lorent, N., Neyrinck, A., Peetermans, M., Thal, D.R., Vandenbriele, C., Wauters, J., Mombaerts, P., Van Gerven, L., 2021b. Visualizing in deceased COVID-19 patients how SARS-CoV-2 attacks the respiratory and olfactory mucosae but spares the olfactory bulb. Cell 184, 5932–5949.e15. https://doi.org/10.1016/j.cell.2021.10.027.

Kim, J., Kim, Y., Kim, H.-T., Kim, D.W., Ha, Y., Kim, J., Kim, C.-H., Lee, I., Song, K., 2009. TC1(C8orf4) Is a Novel Endothelial Inflammatory Regulator Enhancing NF-κB Activity. J. Immunol. 183 (6), 3996–4002. https://doi.org/10.4049/jimmunol.0900956.

Kirschenbaum, D., Imbach, L.L., Ulrich, S., Rushing, E.J., Keller, E., Reimann, R.R., Frauenknecht, K.B.M., Lichtblau, M., Witt, M., Hummel, T., Steiger, P., Aguzzi, A., Frontzek, K., 2020. Inflammatory olfactory neuropathy in two patients with COVID-19. Lancet 396 (10245), 166. https://doi.org/10.1016/S0140-6736(20)31525-7.

Kraemer, A.M., Saraiva, L.R., Korsching, S.I., 2008. Structural and functional diversification in the teleost S100 family of calcium-binding proteins. BMC Evol. Biol. 8 (1) https://doi.org/10.1186/1471-2148-8-48.

Kraus, A., Buckley, K.M., Salinas, I., 2021. Sensing the world and its dangers : An evolutionary perspective in neuroimmunology. Elife 10, e66706. https://doi.org/10.7554/eLife.66706.

Kraus, A., Casadei, E., Huertas, M., Ye, C., Bradfute, S., Boudinot, P., Levraud, J.-P., Salinas, I., 2020. A zebrafish model for COVID-19 recapitulates olfactory and cardiovascular pathophysiologies caused by SARS-CoV-2. bioRxiv. https://doi.org/10.1101/2020.11.06.368191.

Ku, M.-W., Bourgine, M., Authié, P., Lopez, J., Nemirov, K., Moncoq, F., Noirat, A., Vesin, B., Nevo, F., Blanc, C., Souque, P., Tabbal, H., Simon, E., Le Dudal, M.,

Guinet, F., Fiette, L., Mouquet, H., Anna, F., Martin, A., Escriou, N., Majlessi, L., Charneau, P., 2020. Intranasal Vaccination with a Lentiviral Vector Strongly Protects against SARS-CoV-2 in Mouse and Golden Hamster Preclinical Models. BioRxiv. https://doi.org/10.1101/2020.07.21.214049.

Laghi, V., Rezelj, V., Boucontet, L., Frétaud, M., da Costa, B., Boudinot, P., Salinas, I., Lutfalla, G., Vignuzzi, M., Levraud, J.-P., 2021. Exploring zebrafish larvae as a COVID-19 model: probable SARS-COV-2 replication in the swim bladder. BioRxiv. https://doi.org/10.1101/2021.04.08.439059.

Lan, J., Ge, J., Yu, J., Shan, S., Zhou, H., Fan, S., Zhang, Q., Shi, X., Wang, Q., Zhang, L., Wang, X., 2020. Structure of the SARS-CoV-2 spike receptor-binding domain bound to the ACE2 receptor. Nature 581 (7807), 215–220. https://doi.org/10.1038/s41586-020-2180-5.

Laude, H., Gelfi, J., Lavenant, L., Charley, B., 1992. Single amino acid changes in the viral glycoprotein M affect induction of alpha interferon by the coronavirus transmissible gastroenteritis virus. J. Virol. 66 (2), 743–749. https://doi.org/10.1128/jvi.66.2.743-749.1992.

Letarov, A.V., Babenko, V.V., Kulikov, E.E., 2021. Free SARS-CoV-2 Spike Protein S1 Particles May Play a Role in the Pathogenesis of COVID-19 Infection. Biochem. 86 (3), 257–261. https://doi.org/10.1134/S0006297921030032.

Leung, C.T., Coulombe, P.A., Reed, R.R., 2007. Contribution of olfactory neural stem cells to tissue maintenance and regeneration. Nat. Neurosci. 10 (6), 720–726. https://doi.org/10.1038/nn1882.

Levraud, J.-P., Palha, N., Langevin, C., Boudinot, P., 2014. Through the looking glass: witnessing host–virus interplay in zebrafish. Trends Microbiol. 22 (9), 490–497. https://doi.org/10.1016/j.tim.2014.04.014.

Li, L., Chong, H.C., Ng, S.Y., Kwok, K.W., Teo, Z., Tan, E.H.P., Choo, C.C., Seet, J.E., Choi, H.W., Buist, M.L., Chow, V.T.K., Tan, N.S., 2015. Angiopoietin-like 4 increases pulmonary tissue leakiness and damage during influenza pneumonia. Cell Rep. 10 (5), 654–663. https://doi.org/10.1016/j.celrep.2015.01.011.

Liu, Z., Xiao, X., Wei, X., Li, J., Yang, J., Tan, H., Zhu, J., Zhang, Q., Wu, J., Liu, L., 2020. Composition and divergence of coronavirus spike proteins and host ACE2 receptors predict potential intermediate hosts of SARS-CoV-2. J. Med. Virol. 92 (6), 595–601. https://doi.org/10.1002/jmv.v92.610.1002/jmv.25726.

Lucas, C., Wong, P., Klein, J., Castro, T.B.R., Silva, J., Sundaram, M., Ellingson, M.K., Mao, T., Oh, J.E., Israelow, B., Takahashi, T., Tokuyama, M., Lu, P., Venkataraman, A., Park, A., Mohanty, S., Wang, H., Wyllie, A.L., Vogels, C.B.F., Earnest, R., Lapidus, S., Ott, I.M., Moore, A.J., Muenker, M.C., Fournier, J.B., Campbell, M., Odio, C.D., Casanovas-Massana, A., Obaid, A., Lu-Culligan, A., Nelson, A., Brito, A., Nunez, A., Martin, A., Watkins, A., Geng, B., Kalinich, C., Harden, C., Todeasa, C., Jensen, C., Kim, D., McDonald, D., Shepard, D., Courchaine, E., White, E.B., Song, E., Silva, E., Kudo, E., DeIuliis, G., Rahming, H., Park, H.-J., Matos, I., Nouws, J., Valdez, J., Fauver, J., Lim, J., Rose, K.-A., Anastasio, K., Brower, K., Glick, L., Sharma, L., Sewanan, L., Knaggs, L., Minasyan, M., Batsu, M., Petrone, M., Kuang, M., Nakahata, M., Campbell, M., Linehan, M., Askenase, M.H., Simonov, M., Smolgovsky, M., Sonnert, N., Naushad, N., Vijayakumar, P., Martinello, R., Datta, R., Handoko, R., Bermejo, S., Prophet, S., Bickerton, S., Velazquez, S., Alpert, T., Rice, T., Khoury-Hanold, W., Peng, X., Yang, Y., Cao, Y., Strong, Y., Herbst, R., Shaw, A.C., Medzhitov, R., Schulz, W.L., Grubaugh, N.D., Dela Cruz, C., Farhadian, S., Ko, A.I., Omer, S.B., Iwasaki, A., 2020. Longitudinal analyses reveal immunological misfiring in severe COVID-19. Nature 584 (7821), 463–469. https://doi.org/10.1038/s41586-020-2588-y.

Mangia, L.R.L., Soares, M.B., de Souza, T.S.C., De Masi, R.D.João., Scarabotto, Patrícia. C., Hamerschmidt, R., 2021. Objective evaluation and predictive value of olfactory dysfunction among patients hospitalized with COVID-19. Auris Nasus Larynx 48 (4), 770–776. https://doi.org/10.1016/j.anl.2021.01.015.

Martorana, M.L., Tawk, M., Lapointe, T., Barre, N., Imboden, M., Joulie, C., Géraudie, J., Vriz, S., 2001. Zebrafish keratin 8 is expressed at high levels in the epidermis of regenerating caudal fin. Int. J. Dev. Biol. 45, 449–452. https://doi.org/10.1387/ijdb.11330866.

Meisel, J.D., Kim, D.H., 2014. Behavioral avoidance of pathogenic bacteria by Caenorhabditis elegans. Trends Immunol. 35 (10), 465–470. https://doi.org/10.1016/j.it.2014.08.008.

Mellert, T.K., Getchell, M.L., Sparks, L., Getchell, T.V., 1992. Characterization of the immune barrier in human olfactory mucosa. Otolaryngol Head Neck Surg. 106 (2), 181–188.

Michel, W.C., Derbidge, D.S., 1997. Evidence of distinct amino acid and bile salt receptors in the olfactory system of the zebrafish. Danio rerio. Brain Res. 764 (1-2), 179–187. https://doi.org/10.1016/S0006-8993(97)00454-X.

Muus, C., Luecken, M.D., Eraslan, Gökcen, Sikkema, L., Waghray, A., Heimberg, G., Kobayashi, Y., Vaishnav, E.D., Subramanian, A., Smillie, C., Jagadeesh, K.A., Duong, E.T., Fiskin, E., Triglia, E.T., Ansari, M., Cai, P., Lin, B., Buchanan, J., Chen, S., Shu, J., Haber, A.L., Chung, H., Montoro, D.T., Adams, T., Aliee, H., Allon, S.J., Andrusivova, Z., Angelidis, I., Ashenberg, O., Bassler, K., Bécavin, C., Benhar, I., Bergenstråhle, J., Bergenstråhle, L., Bolt, L., Braun, E., Bui, L.T., Callori, S., Chaffin, M., Chichelnitskiy, E., Chiou, J., Conlon, T.M., Cuoco, M.S., Cuomo, A.S.E., Deprez, M., Duclos, G., Fine, D., Fischer, D.S., Ghazanfar, S., Gillich, A., Giotti, B., Gould, J., Guo, M., Gutierrez, A.J., Habermann, A.C., Harvey, T., He, P., Hou, X., Hu, L., Hu, Y., Jaiswal, A., Ji, L., Jiang, P., Kapellos, T.S., Kuo, C.S., Larsson, L., Leney-Greene, M.A., Lim, K., Litviňuková, M., Ludwig, L.S., Lukassen, S., Luo, W., Maatz, H., Madissoon, E., Mamanova, L., Manakongtreecheep, K., Leroy, S., Mayr, C.H., Mbano, I.M., McAdams, A.M., Nabhan, A.N., Nyquist, S.K., Penland, L., Poirion, O.B., Poli, S., Qi, C., Queen, R., Reichart, D., Rosas, I., Schupp, J.C., Shea, C.V., Shi, X., Sinha, R., Sit, R.V., Slowikowski, K., Slyper, M., Smith, N.P., Sountoulidis, A., Strunz, M., Sullivan, T.B., Sun, D., Talavera-López, C., Tan, P., Tantivit, J., Travaglini, K.J., Tucker, N.R.,

Vernon, K.A., Wadsworth, M.H., Waldman, J., Wang, X., Xu, K., Yan, W., Zhao, W., Ziegler, C.G.K., 2021. Single-cell meta-analysis of SARS-CoV-2 entry genes across tissues and demographics. Nat. Med. 27 (3), 546–559. https://doi.org/10.1038/s41591-020-01227-z.

Paladini, R.D., Takahashi, K., Bravo, N.S., Coulombe, P.A., 1996. Onset of re-epithelialization after skin injury correlates with a reorganization of keratin filaments in wound edge keratinocytes: Defining a potential role for keratin 16. J. Cell Biol. 132, 381–397. https://doi.org/10.1083/jcb.132.3.381.

Parma, V., Ohla, K., Veldhuizen, M.G., Niv, M.Y., Kelly, C.E., Bakke, A.J., Cooper, K.W., Bouysset, C., Pirastu, N., Dibattista, M., Kaur, R., Liuzza, M.T., Pepino, M.Y., Schöpf, V., Pereda-Loth, V., Olsson, S.B., Gerkin, R.C., Rohlfs Domínguez, P., Albayay, J., Farruggia, M.C., Bhutani, S., Fjaeldstad, A.W., Kumar, R., Menini, A., Bensafi, M., Sandell, M., Konstantinidis, I., Di Pizio, A., Genovese, F., Öztürk, L., Thomas-Danguin, T., Frasnelli, J., Boesveldt, S., Saatci, Ö., Saraiva, L.R., Lin, C., Golebiowski, J., Hwang, L.-D., Ozdener, M.H., Guàrdia, M.D., Laudamiel, C., Ritchie, M., Havlícek, J., Pierron, D., Roura, E., Navarro, M., Nolden, A.A., Lim, J., Whitcroft, K.L., Colquitt, L.R., Ferdenzi, C., Brindha, E.V, Altundag, A., Macchi, A., Nunez-Parra, A., Patel, Z.M., Fiorucci, S., Philpott, C.M., Smith, B.C., Lundström, J.N., Mucignat, C., Parker, J.K., van den Brink, M., Schmuker, M., Fischmeister, F.P.S., Heinbockel, T., Shields, V.D.C., Faraji, F., Santamaría, E., Fredborg, W.E.A., Morini, G., Olofsson, J. K., Jalessi, M., Karni, N., D'Errico, A., Alizadeh, R., Pellegrino, R., Meyer, P., Huart, C., Chen, B., Soler, G.M., Alwashahi, M.K., Welge-Lüssen, A., Freiherr, J., de Groot, J. H.B., Klein, H., Okamoto, M., Singh, P.B., Hsieh, J.W., GCCR Group Author, Reed, D. R., Hummel, T., Munger, S.D., Hayes, J.E., 2020. More Than Smell—COVID-19 Is Associated With Severe Impairment of Smell, Taste, and Chemesthesis. Chem. Senses 45, 609–622. doi:org/10.1093/chemse/bjaa041.

Palha, N., Guivel-Benhassine, F., Briolat, V., Lutfalla, G., Sourisseau, M., Ellett, F., Wang, C.-H., Lieschke, G.J., Herbomel, P., Schwartz, O., Levraud, J.-P., Heise, M.T., 2013. Real-Time Whole-Body Visualization of Chikungunya Virus Infection and Host Interferon Response in Zebrafish. PLoS Pathog. 9 (9), e1003619. https://doi.org/10.1371/journal.ppat.1003619.

Papadakis, K.A., Landers, C., Prehn, J., Kouroumalis, E.A., Moreno, S.T., Gutierrez-Ramos, J.-C., Hodge, M.R., Targan, S.R., 2003. CC Chemokine Receptor 9 Expression Defines a Subset of Peripheral Blood Lymphocytes with Mucosal T Cell Phenotype and Th1 or T-Regulatory 1 Cytokine Profile. J. Immunol. 171 (1), 159–165. https://doi.org/10.4049/jimmunol.171.1.159.

Patra, T., Meyer, K., Geerling, L., Isbell, T.S., Hoft, D.F., Brien, J., Pinto, A.K., Ray, R.B., Ray, R., Lee, B., 2020. SARS-CoV-2 spike protein promotes IL-6 transsignaling by activation of angiotensin II receptor signaling in epithelial cells. PLoS Pathog. 16 (12), e1009128. https://doi.org/10.1371/journal.ppat.1009128.

Peterson, J., Lin, B., Barrios-Camacho, C.M., Herrick, D.B., Holbrook, E.H., Jang, W., Coleman, J.H., Schwob, J.E., 2019. Activating a Reserve Neural Stem Cell Population In Vitro Enables Engraftment and Multipotency after Transplantation. Stem Cell Reports 12, 680–695. https://doi.org/10.1016/j.stemcr.2019.02.014.

Pfaffl, M.W., 2001. A new mathematical model for relative quantification in real-time RT–PCR. Nucleic Acids Res. 29 https://doi.org/10.1111/j.1365-2966.2012.21196.x.

Pozharskaya, T., Liang, J., Lane, A.P., 2013. Regulation of inflammation-associated olfactory neuronal death and regeneration by the type II tumor necrosis factor receptor. Int. Forum Allergy Rhinol. 3 (9), 740–747. https://doi.org/10.1002/alr.21187.

Raghavan, S., Kenchappa, D.B., Leo, M.D., 2021. SARS-CoV-2 Spike Protein Induces Degradation of Junctional Proteins That Maintain Endothelial Barrier Integrity. Front. Cardiovasc. Med. 8, 687783 https://doi.org/10.3389/fcvm.2021.687783.

Rahimzadeh, M., Naderi, N., 2021. Toward an understanding of regulatory T cells in COVID-19: A systematic review. J. Med. Virol. 93, 4167–4181. https://doi.org/10.1002/jmv.26891.

Rapid Deployment Vaccine Collaborative (RaDVaC), 2021. SARS-CoV-2 (2019-nCoV) vaccine [White page].

Rhea, E.M., Logsdon, A.F., Hansen, K.M., Williams, L.M., Reed, M.J., Baumann, K.K., Holden, S.J., Raber, J., Banks, W.A., Erickson, M.A., 2021. The S1 protein of SARS-CoV-2 crosses the blood–brain barrier in mice. Nat. Neurosci. 24 (3), 368–378. https://doi.org/10.1038/s41593-020-00771-8.

Rodriguez, S., Cao, L., Rickenbacher, G.T., Benz, E.G., Magdamo, C., Gomez, L.R., Holbrook, E.H., Albers, A.D., Gallagher, R., Westover, M.B., Evans, K.E., Tatar, D.J., Mukerji, S., Zafonte, R., Boyer, E.W., Yu, C.R., Albers, M.W., 2020. Innate immune signaling in the olfactory epithelium reduces odorant receptor levels: modeling transient smell loss in COVID-19 patients. MedRxiv. https://. https://doi.org/10.1101/2020.06.14.20131128.

Sahoo, P.K., Aparna, S., Naik, P.K., Singh, S.B., Das, S.K., 2021. Bisphenol A exposure induces neurobehavioral deficits and neurodegeneration through induction of oxidative stress and activated caspase-3 expression in zebrafish brain. J Biochem Mol Toxicol 35 (10). https://doi.org/10.1002/jbt.v35.1010.1002/jbt.22873.

Saraiva, L.R., Ahuja, G., Ivandic, I., Syed, A.S., Marioni, J.C., Korsching, S.I., Logan, D. W., 2015. Molecular and neuronal homology between the olfactory systems of zebrafish and mouse. Sci. reports 5, 11487. https://doi.org/10.1038/srep11487.

Sarkar, S.K., Jana, S., Barman, S., Kumar De, S., 2018. Age-related Cytological Changes of Fibroblast Cell and Fila Olfactoria in Fish: [Pseudapocryptes lanceolatus (Bloch and Schneider)]. Microsc. Microanal. 24 (S1), 1304–1305. https://doi.org/10.1017/S1431927618007006.

Sato, Y., Miyasaka, N., Yoshihara, Y., 2005. Mutually Exclusive Glomerular Innervation by Two Distinct Types of Olfactory Sensory Neurons Revealed in Transgenic Zebrafish. J. Neurosci. 25, 4889–4897. https://doi.org/10.1523/jneurosci.0679-05.2005.

Sbrana, M.F., Fornazieri, M.A., Bruni-Cardoso, A., Avelino-Silva, V.I., Schechtman, D., Voegels, R.L., Malnic, B., Glezer, I., de Rezende Pinna, F., 2021. Olfactory

Dysfunction in Frontline Health Care Professionals During COVID-19 Pandemic in Brazil. Front. Physiol. 12, 622987 https://doi.org/10.3389/fphys.2021.622987.

Sepahi, A., Kraus, A., Casadei, E., Johnston, C.A., Galindo-villegas, J., Kelly, C., García-Morenoc, D., Muñoze, P., Mulero, V., Huertas, M., Salinas, I., ACenter, 2019. Olfactory sensory neurons mediate ultrarapid antiviral immune responses in a TrkA-dependent manner. PNAS 116, 12428–12436. https://doi.org/10.1073/pnas.1900083116.

Sepahi, A., Tacchi, L., Casadei, E., Takizawa, F., LaPatra, S.E., Salinas, I., 2017. CK12a, a CCL19-like Chemokine That Orchestrates both Nasal and Systemic Antiviral Immune Responses in Rainbow Trout. J. Immunol. 199 (11), 3900–3913. https://doi.org/10.4049/jimmunol.1700757.

Slade, C.D., Reagin, K.L., Lakshmanan, H.G., Klonowski, K.D., Watford, W.T., Varga, S. M., 2020. Placenta-specific 8 limits IFNγ production by CD4 T cells in vitro and promotes establishment of influenza-specific CD8 T cells in vivo. PLoS One 15 (7), e0235706. https://doi.org/10.1371/journal.pone.0235706.

Song, E., Zhang, C., Israelow, B., Lu-Culligan, A., Prado, A.V., Skriabine, S., Lu, P., Weizman, O.E., Liu, F., Dai, Y., Szigeti-Buck, K., Yasumoto, Y., Wang, G., Castaldi, C., Heltke, J., Ng, E., Wheeler, J., Alfajaro, M.M., Levavasseur, E., Fontes, B., Ravindra, N.G., van Dijk, D., Mane, S., Gunel, M., Ring, A., Jaffar Kazmi, S.A., Zhang, K., Wilen, C.B., Horvath, T.L., Plu, I., Haik, S., Thomas, J.L., Louvi, A., Farhadian, S.F., Huttner, A., Seilhean, D., Renier, N., Bilguvar, K., Iwasaki, A., 2021. Neuroinvasion of SARS-CoV-2 in human and mouse brain. J. Exp. Med. 218, e20202135 https://doi.org/10.1084/JEM.20202135.

Spinato, G., Fabbris, C., Polesel, J., Cazzador, D., Borsetto, D., Hopkins, C., Boscolo-Rizzo, P., 2020. Alterations in Smell or Taste in Mildly Symptomatic Outpatients With SARS-CoV-2 Infection. N. Engl. J. Med. 323, 2005–2011. https://doi.org/10.1056/nejmoa2005412.

Stensmyr, M.C., Dweck, H.K.M., Farhan, A., Ibba, I., Strutz, A., Mukunda, L., Linz, J., Grabe, V., Steck, K., Lavista-Llanos, S., Wicher, D., Sachse, S., Knaden, M., Becher, P. G., Seki, Y., Hansson, B.S., 2012. A conserved dedicated olfactory circuit for detecting harmful microbes in drosophila. Cell 151 (6), 1345–1357. https://doi.org/10.1016/j.cell.2012.09.046.

Sungnak, W., Huang, N., Bécavin, C., Berg, M., Queen, R., Litvinukova, M., Talavera-López, C., Maatz, H., Reichart, D., Sampaziotis, F., Worlock, K.B., Yoshida, M., Barnes, J.L., Banovich, N.E., Barbry, P., Brazma, A., Collin, J., Desai, T.J., Duong, T. E., Eickelberg, O., Falk, C., Farzan, M., Glass, I., Gupta, R.K., Haniffa, M., Horvath, P., Hubner, N., Hung, D., Kaminski, N., Krasnow, M., Kropski, J.A., Kuhnemund, M., Lako, M., Lee, H., Leroy, S., Linnarson, S., Lundeberg, J., Meyer, K. B., Miao, Z., Misharin, A.V., Nawijn, M.C., Nikolic, M.Z., Noseda, M., Ordovas-Montanes, J., Oudit, G.Y., Pe'er, D., Powell, J., Quake, S., Rajagopal, J., Tata, P.R., Rawlins, E.L., Regev, A., Reyfman, P.A., Rozenblatt-Rosen, O., Saeb-Parsy, K., Samakovlis, C., Schiller, H.B., Schultze, J.L., Seibold, M.A., Seidman, C.E., Seidman, J.G., Shalek, A.K., Shepherd, D., Spence, J., Spira, A., Sun, X., Teichmann, S.A., Theis, F.J., Tsankov, A.M., Vallier, L., van den Berge, M., Whitsett, J., Xavier, R., Xu, Y., Zaragosi, L.E., Zerti, D., Zhang, H., Zhang, K., Rojas, M., Figueiredo, F., 2020. SARS-CoV-2 entry factors are highly expressed in nasal epithelial cells together with innate immune genes. Nat. Med. 26, 681–687. https://doi.org/10.1038/s41591-020-0868-6.

Suzukawa, K., Kondo, K., Kanaya, K., Sakamoto, T., Watanabe, K., Ushio, M., Kaga, K., Yamasoba, T., 2011. Age-related changes of the regeneration mode in the mouse peripheral olfactory system following olfactotoxic drug methimazole-induced damage. J. Comp. Neurol. 519 (11), 2154–2174. https://doi.org/10.1002/cne.22611.

Suzuki, M., Saito, K., Min, W.-P., Vladau, C., Toida, K., Itoh, H., Murakami, S., 2007. Identification of viruses in patients with postviral olfactory dysfunction. Laryngoscope 117 (2), 272–277. https://doi.org/10.1097/01.mlg.0000249922.37381.1e.

Tacchi, L., Musharrafieh, R., Larragoite, E.T., Crossey, K., Erhardt, E.B., Martin, S.A.M., LaPatra, S.E., Salinas, I., 2014. Nasal immunity is an ancient arm of the mucosal immune system of vertebrates. Nat. Commun. 5, 5205. https://doi.org/10.1038/ncomms6205.

Theobald, S.J., Simonis, A., Georgomanolis, T., Kreer, C., Zehner, M., Eisfeld, H.S., Albert, M., Chhen, J., Motameny, S., Erger, F., Fischer, J., Malin, J.J., Gräb, J., Winter, S., Pouikli, A., David, F., Böll, B., Koehler, P., Vanshylla, K., Gruell, H., Suárez, I., Hallek, M., Fätkenheuer, G., Jung, N., Cornely, O.A., Lehmann, C., Tessarz, P., Altmüller, J., Nürnberg, P., Kashkar, H., Klein, F., Koch, M., Rybniker, J., 2021. Long-lived macrophage reprogramming drives spike protein-mediated inflammasome activation in COVID-19. EMBO Mol. Med. 16, e14150 https://doi.org/10.15252/emmm.202114150.

Tian, S., Xiong, Y., Liu, H., Niu, L., Guo, J., Liao, M., Xiao, S.-Y., 2020. Pathological study of the 2019 novel coronavirus disease (COVID-19) through postmortem core biopsies. Mod. Pathol. 33 (6), 1007–1014. https://doi.org/10.1038/s41379-020-0536-x.

Torabi, A., Mohammadbagheri, E., Akbari Dilmaghani, N., Bayat, A.-H., Fathi, M., Vakili, K., Alizadeh, R., Rezaeimirghaed, O., Hajiesmaeili, M., Ramezani, M., Simani, L., Aliaghaei, A., 2020. Proinflammatory Cytokines in the Olfactory Mucosa Result in COVID-19 Induced Anosmia. ACS Chem. Neurosci. 11 (13), 1909–1913. https://doi.org/10.1021/acschemneuro.0c00249.

Tyrkalska, S.D., Martínez-López, A., Arroyo, A.B., Martínez-Morcillo, F.J., Candel, S., García-Moreno, D., Mesa-del-Castillo, P., Cayuela, M.L., Mulero, V., 2021. A zebrafish model of COVID-19-associated cytokine storm syndrome reveals differential proinflammatory activities of Spike proteins of SARS-CoV-2 variants of concern. BioRxiv. https://. https://doi.org/10.1101/2021.12.05.471277.

Urata, S., Maruyama, J., Kishimoto-Urata, M., Sattler, R.A., Cook, R., Lin, N., Yamasoba, T., Makishima, T., Paessler, S., 2021. Regeneration Profiles of Olfactory

Epithelium after SARS-CoV-2 Infection in Golden Syrian Hamsters. ACS Chem. Neurosci. 12 (4), 589–595. https://doi.org/10.1021/acschemneuro.0c00649.s001.

Usui, M.L., Underwood, R.A., Mansbridge, J.N., Muffley, L.A., Carter, W.G., Olerud, J.E., 2005. Morphological evidence for the role of suprabasal keratinocytes in wound reepithelialization. Wound Repair Regen. 13, 468–479. https://doi.org/10.1111/j.1067-1927.2005.00067.x.

Van Doremalen, N., Purushotham, J.N., Schulz, J.E., Holbrook, M.G., Bushmaker, T., Carmody, A., Port, J.R., Yinda, C.K., Okumura, A., Saturday, G., Amanat, F., Krammer, F., Hanley, P.W., Smith, B.J., Lovaglio, J., Anzick, S.L., Barbian, K., Martens, C., Gilbert, S.C., Lambe, T., Munster, V.J., 2021. Intranasal ChAdOx1 nCoV-19 / AZD1222 vaccination reduces viral shedding after SARS-CoV-2 D614G challenge in preclinical models. Sci. Transl. Med. 13, eabh0755.

Van Dycke, J., Ny, A., Conceição-Neto, Nádia, Maes, J., Hosmillo, M., Cuvry, A., Goodfellow, I., Nogueira, T.C., Verbeken, E., Matthijnssens, J., de Witte, P., Neyts, J., Rocha-Pereira, J., Suthar, M., 2019. A robust human norovirus replication model in zebrafish larvae. PLoS Pathog. 15 (9), e1008009. https://doi.org/10.1371/journal.ppat.1008009.

Ventura Fernandes, B.H., Feitosa, N.M., Barbosa, A.P., Bomfim, C.G., Garnique, A.M.B., Rosa, I.F., Rodrigues, M.S., Doretto, L.B., Costa, D.F., Camargo-Dos-Santos, B., Franco, G.A., Neto, J.F., Lunardi, J.S., Bellot, M.S., Alves, N.P.C., Costa, C.C., Aracati, M.F., Rodrigues, L.F., Costa, C.C., Cirilo, R.H., Colagrande, R.M., Gomes, F.I. F., Nakajima, R.T., Belo, M.A.A., Giaquinto, P.C., de Oliveira, S.L., Eto, S.F., Fernandes, D.C., Manrique, W.G., Conde, G., Rosales, R.R.C., Todeschini, I., Rivero, I., Llontop, E., Sgro, G.G., Oka, G.U., Bueno, N.F., Ferraris, F.K., de Magalhães, M.T.Q., Medeiros, R.J., Mendonça-Gomes, J.M., Junqueira, M.S., Conceição, K., Pontes, L.G., Condino-Neto, A., Perez, A.C., Barcellos, L.J.G., Júnior, J.D.C., Dorlass, E.G., Camara, N.O.S., Durigon, E.L., Cunha, F.Q., Nóbrega, R. H., Machado-Santelli, G.M., Farah, C.S., Veras, F.P., Galindo-Villegas, J., Costa-Lotufo, L.V., Cunha, T.M., Chammas, R., Carvalho, L.R., Guzzo, C.R., Malafaia, G., Charlie-Silva, I., 2022 Mar. Toxicity of spike fragments SARS-CoV-2 S protein for zebrafish: A tool to study its hazardous for human health? Sci Total Environ. 20 (813), 152345 https://doi.org/10.1016/j.scitotenv.2021.152345.

Waggener, C.T., Coppola, D.M., 2007. Naris occlusion alters the electro-olfactogram: Evidence for compensatory plasticity in the olfactory system. Neurosci. Let. 427 (2), 112–116. https://doi.org/10.1016/j.neulet.2007.09.013.

Wagener, B.M., Hu, M., Zheng, A., Zhao, X., Che, P., Brandon, A., Anjum, N., Snapper, S., Creighton, J., Guan, J.-L., Han, Q., Cai, G.-Q., Han, X., Pittet, J.-F., Ding, Q., 2016. Neuronal Wiskott–Aldrich syndrome protein regulates TGF-β1–mediated lung vascular permeability. FASEB J 34, 3305–3317. https://doi.org/doi: 10.1096/fj.201902915R.

Wang, S., Guo, F., Liu, K., Wang, H., Rao, S., Yang, P., Jiang, C., 2008. Endocytosis of the receptor-binding domain of SARS-CoV spike protein together with virus receptor ACE2. Virus Res. 136 (1-2), 8–15. https://doi.org/10.1016/j.virusres.2008.03.004.

Wei, S., Zhou, J.-min., Chen, X., Shah, R.N., Liu, J., Orcutt, T.M., Traver, D., Djeu, J.Y., Litman, G.W., Yoder, J.A., 2007. The zebrafish activating immune receptor Nitr9 signals via Dap12. Immunogenetics 59 (10), 813–821. https://doi.org/10.1007/s00251-007-0250-6.

White, E.J., Kounelis, S.K., Byrd-Jacobs, C.A., 2015. Plasticity of Glomeruli and Olfactory-Mediated Behavior in Zebrafish Following Detergent Lesioning of the Olfactory Epithelium. Neuroscience 284, 622–631. https://doi.org/10.1016/j.neuroscience.2014.10.036.

Xu, Z., Shi, L., Wang, Y., Zhang, J., Huang, L., Zhang, C., Liu, S., Zhao, P., Liu, H., Zhu, L., Tai, Y., Bai, C., Gao, T., Song, J., Xia, P., Dong, J., Zhao, J., Wang, F.-S., 2020. Pathological findings of COVID-19 associated with acute respiratory distress syndrome. Lancet Respir. Med. 8 (4), 420–422. https://doi.org/10.1016/S2213-2600(20)30076-X.

Yang, A.C., Kern, F., Losada, P.M., Agam, M.R., Maat, C.A., Schmartz, G.P., Fehlmann, T., Stein, J.A., Schaum, N., Lee, D.P., Calcuttawala, K., Vest, R.T., Berdnik, D., Lu, N., Hahn, O., Gate, D., McNerney, M.W., Channappa, D., Cobos, I., Ludwig, N., Schulz-Schaeffer, W.J., Keller, A., Wyss-Coray, T., 2021. Dysregulation of brain and choroid plexus cell types in severe COVID-19. Nature 595 (7868), 565–571. https://doi.org/10.1038/s41586-021-03710-0.

Yao, Y., Yao, J., Boström, K.I., 2019. SOX Transcription Factors in Endothelial Differentiation and Endothelial-Mesenchymal Transitions. Front. Cardiovasc. Med. 6, 30. https://doi.org/10.3389/fcvm.2019.00030.

Yoo, S.K., Huttenlocher, A., 2011. Spatiotemporal photolabeling of neutrophil trafficking during inflammation in live zebrafish. J. Leukoc. Biol. 89 (5), 661–667. https://doi.org/10.1189/jlb.1010567.

Yu, C.R., Wu, Y., 2017. Regeneration and rewiring of rodent olfactory sensory neurons. Exp. Neurol. 287, 395–408. https://doi.org/10.1016/j.expneurol.2016.06.001.

Zazhytska, M., Kodra, A., Hoagland, D.A., Fullard, J.F., Shayya, H., Omer, A., Firestein, S., Gong, Q., Canoll, P.D., Goldman, J.E., Roussos, P., TenOever, B.R., Overdevest, J.B., Lomvardas, S., 2021. Disruption of nuclear architecture as a cause of COVID-19 induced anosmia. BioRxiv. https://. https://doi.org/10.1101/2021.02.09.430314.

Zhang, A.J., Lee, A.C.-Y., Chu, H., Chan, J.F.-W., Fan, Z., Li, C., Liu, F., Chen, Y., Yuan, S., Poon, V.K.-M., Chan, C.C.-S., Cai, J.-P., Wu, K.L.-K., Sridhar, S., Chan, Y.-S., Yuen, K.-Y., 2020. Severe Acute Respiratory Syndrome Coronavirus 2 Infects and Damages the Mature and Immature Olfactory Sensory Neurons of Hamsters. Clin. Infect. Dis. Jul 15, ciaa995. https://doi.org/10.1093/cid/ciaa995.

Zheng, J., Wong, L.-Y., Li, K., Verma, A.K., Ortiz, M.E., Wohlford-Lenane, C., Leidinger, M.R., Knudson, C.M., Meyerholz, D.K., McCray, P.B., Perlman, S., 2020. COVID-19 treatments and pathogenesis including anosmia in K18-hACE2 mice. Nature 589 (7843), 603–607. https://doi.org/10.1038/s41586-020-2943-z.

Zheng, L., Ma, Y., Chen, M., Wu, G., Yan, C., Zhang, X.-E., 2021. Biochemical and Biophysical Research Communications SARS-CoV-2 spike protein receptor-binding domain N-glycans facilitate viral internalization in respiratory epithelial cells. Biochem. Biophys. Res. Commun. 579, 69–75. https://doi.org/10.1016/j.bbrc.2021.09.053.

Zheng, Y., Vertuani, S., Nyström, S., Audebert, S., Meijer, I., Tegnebratt, T., Borg, J.-P., Uhlén, P., Majumdar, A., Holmgren, L., 2009. Angiomotin-like protein 1 controls endothelial polarity and junction stability during sprouting angiogenesis. Circ. Res. 105 (3), 260–270. https://doi.org/10.1161/CIRCRESAHA.109.195156.

Zhou, Y., Zhou, B., Pache, L., Chang, M., Khodabakhshi, A.H., Tanaseichuk, O., Benner, C., Chanda, S.K., 2019. Metascape provides a biologist-oriented resource for the analysis of systems-level datasets. Nat. Commun. 10 (1) https://doi.org/10.1038/s41467-019-09234-6.

Zou, J., Secombes, C., 2016. The function of fish cytokines. Biology (Basel). 5 (2), 23. https://doi.org/10.3390/biology5020023.

Zuo, W., Zhao, X., Chen, Y.-G., 2010. In: Molecular Biology of the SARS-Coronavirus. Springer Berlin Heidelberg, Berlin, Heidelberg, pp. 247–258. https://doi.org/10.1007/978-3-642-03683-5_15.